Shifts in embryonic oxygen levels cue heterochrony in limb initiation

Meng Zhu[1], Rinaldo Catta-Preta[1,2,3], ChangHee Lee[1], Clifford Tabin[1,*]

[1] Department of Genetics, Blavatnik Institute, Harvard Medical School, United States of America

[2] Ocular Genomics Institute, Massachusetts Eye and Ear, Boston, United States of America

[3] Department of Ophthalmology, Harvard Medical School, Boston, United States of America

[*]Correspondence to: tabin@genetics.med.harvard.edu

Abstract (125 words)

Heterochrony, or the alteration of developmental timing, is an important mechanism of evolutionary change. Avian species display synchronized growth of the forelimbs and hindlimbs, while mammalian species show delayed hindlimb development. We find that mammalian limb heterochrony is evident from the start of limb bud formation, and is associated with heterochronic expression of T-box transcription factors. This heterochronic shift is not due to changes in cis-regulatory sequences controlling T-box gene expression, but unexpectedly, is dependent upon differential oxygen levels to which avian and mammalian embryos are exposed prior to limb initiation, mediated, at least partially, by an NFKB transcription factor, cRel. Together, these results provide mechanistic understanding of an important example of developmental heterochrony and exemplify how the maternal environment regulates timing during embryonic development.

Introduction

Tetrapod species have two pairs of limbs that are localized at rostral (forelimb) and caudal (hindlimb) positions along the trunk. Although the two pairs of appendages follow the same general developmental blueprint, they display differences in temporal pattern that align with evolutionary lineages(*1*). A particular interesting case is the amniote clade, where avians and mammals demonstrate disparate temporal dynamics in limb development. In avian species, the early embryonic stages of limb outgrowth are synchronized; while in mammalian species, the hindlimb develops much later than that of the forelimb(*1*). The extent of this heterochrony varies among mammals such that the non-placental mammals display a more pronounced delay than placental mammals, and among the non-placental marsupial species, the ones that have shorter gestation time exhibit higher levels of heterochrony. This heterochronic delay in hindlimb development in mammals has been postulated to represent an "energy trade-off" strategy (*2, 3*), which prioritizes the growth of immediately required structures in the context of limited nutrient availability during early developmental stages. However, a molecular-level understanding of limb

heterochrony regulation remains entirely unsolved. Indeed, in a more general sense, the control of timing during development is vastly under-studied relative to the control of spatially localized gene expression.

We here investigate the molecular basis of limb heterochrony between avian and mammalian species. We find that limb heterochrony in mammals starts at the limb initiation stage. The delayed onset of hindlimb development can be correlated to expression of *Tbx4*, a transcription factor known to regulate the first steps of hindlimb formation. By coupling RNA-sequencing analyses with gain-of-function screens, we identify a repressive role of the NFKB transcription factor cRel in regulating Tbx4 expression. Unexpectedly, we found that the low oxygen levels that early mammalian embryos experience, a by-product of viviparity, causes upregulation of cRel and attenuates Tbx4 expression in mammalian hindlimb tissues. Our study presents the first mechanistic understanding of mammalian limb heterochrony, and illustrates how the maternal environment can instruct timing of tissue development in the foetus.

Results

Limb heterochrony in mammals starts at the epithelial-to-mesenchymal transition

To interrogate the regulation of limb heterochrony, we first characterized the timing of the earliest steps of limb development in both chick and mouse embryos. Both species initiate limb formation by an epithelial-to-mesenchymal transition (EMT) of cells residing in lateral plate mesoderm (LPM). This leads to the emergence of the paddle-like limb bud, and culminates in the patterning and differentiation of limb progenitor cells into the connective tissues and cartilages. To better understand the stage at which limb heterochrony initially occurs, we first compared the timing of EMT. Our previous work established that the EMT in the chicken embryo takes place in the limb fields at HH12-13 in the forelimb, and HH13-14 in the hindlimb (*4*). For the mouse, EMT in the

forelimb was characterized as occurring between E8.5 and E8.75 (*4*). We expanded the analyses to the mouse hindlimb by examining E9.0-E10.0 mouse embryos. We found that at E9.5, majority of the cells in the hindlimb forming regions still remained epithelial, as indicated by polarized F-actin and Laminin(*4*) and a monolayer organization in the LPM epithelium (Fig. 1a). By contrast, at E9.75, most cells in the hindlimb region showed mesenchymal morphology, with unpolarized distribution of both F-actin and Laminin and the multi-layer stacking of unorganized cells (Fig. 1a). These results thus show that EMT initiating the hindlimb in mouse embryos occurs between E9.5 and E9.75. Together with previous results, quantifications pointed to a 2-hour difference in EMT timing between forelimb and hindlimb in chicken embryos, in contrast to an 18-hour difference in mice, thus, tracing limb heterochrony in mammals back to the EMT stage of limb development (Fig. 1b).

The heterochrony in EMT correlates with timing of expression of T-box transcription factors

We hypothesized that the discrepancy in timing of EMT between mouse and chicken embryos would be attributable to the heterochronic expression of key limb initiation regulators. To explore this hypothesis, we analyzed the transcriptional dynamics of signalling pathway ligands and transcription factors previously described as regulating limb initiation, including Fgf10, Wnt8c, Wnt2b, Tbx5 and Tbx4 (*5-10*). Fgf10 and Wnt2b act downstream of Tbx5 to initiate forelimb EMT, while Fgf10 and Wnt8c act downstream of Tbx4 to initiate hindlimb EMT(*6*). To precisely determine their temporal correlation to the timing of EMT, we utilized Hybridization Chain Reaction (HCR) (*11*), a single molecule fluorescence in situ hybridization technology, to visualize transcripts of each gene and to determine their expression dynamics at spatial and temporal resolution. The designed probes show high specificity to the genes of interest as the expression profiles were consistent with results obtained using other methods (*5, 12, 13*) (Fig. 1c,e,g, Fig. S1a-d).

Our analysis across developmental stages in the forelimb and hindlimb regions of chicken and mouse embryos revealed that the dynamics of the T-box transcription factors, Tbx5 and Tbx4, exhibited the strongest correlation with the timing of EMT (Fig. 1c-f; Fig. S1e-f). Specifically, we found that the time when EMT occurs consistently corresponds to the time when half-maximum levels of the Tbx5 or Tbx4 transcripts are reached in the limb mesenchyme of both species (Fig. 1d,f), a correlation not seen with the other genes tested. Furthermore, we found that this correlation is reflected at the cellular level: cells that transit earlier to the mesenchymal state display higher levels of Tbx5/4 transcripts than those yet to transit (Fig. 1g-i). Together, these results suggest T-box transcription factors as the plausible regulators of EMT heterochrony.

Genetic studies show that the depletion of Tbx5 or Tbx4 results in forelimb or hindlimb outgrowth defects, while their overexpression can induce ectopic limb growth (*8, 9, 12, 14, 15*). To directly test whether Tbx5/4 expression regulates the timing of limb, we examined mouse embryos deficient for each of these genes. We had previously shown that depletion of Tbx5 impairs forelimb EMT(*4*). We therefore turned our attention to the established Tbx4 knockout mouse line (*9*). At E9.75, the cells in hindlimb regions of heterozygous Tbx4 knockout embryos have already undergone EMT, as characterized by the localization of F-actin and Laminin. In contrast, a significant proportion of cells in the Tbx4 null embryos remained epithelized and localized to the basal region of the LPM (Fig. S2a-c). These results, together with the previous studies, show that the limb EMT heterochrony in the mouse embryo is associated with the heterochronic expression of Tbx5 and Tbx4.

Expression of upstream activators of Tbx4 is concordant between chicken and mouse embryos

To investigate the mechanisms leading to delayed Tbx4 expression in the mouse embryo, we started by examining the dynamics of the signaling pathways and transcription factors known to regulate the activation of Tbx4 expression. As gastrulation commences, the genes in the Hox clusters are expressed in a 3' to 5' order , resulting in the segmented anterior-posterior patterning of the trunk (*16*). The forelimb regions are marked by expression of Hox4 paralogues, while the hindlimb regions are specified by Hox9 paralogues (*17, 18*). Interactions with a set of signaling pathways involving Bone Morphogenetic Protein (BMP) activity, Wnt activity, and the inhibition of Retinoic acid (RA) are also required for the specification of posterior LPM (*19, 20*). These inputs together activate expression of the transcription factors Pitx1 and Isl1 that are enriched in posterior LPM marking the regions that form the prospective hindlimb (*21-23*). The knockout of each of these transcription factors in the mouse embryo leads to downregulation of Tbx4 at the hindlimb initiation stage (*24-26*).

We first examined signaling activities essential for LPM specification. Existing literature does not support any notable disparities in the timing of Wnt or RA activation between the mouse and chick (*27-30*). Additionally, our examination of the temporal and spatial distribution of phosphorylated Smad proteins, indicators of BMP pathway activation, revealed no discernible differences between species (Fig. 2a-b). Thus, there do not appear to be temporal alterations in signaling pathways required to specify the hindlimb in the two species.

We then probed the transcriptional dynamics of Hoxb9, Pitx1 and Isl1 expression in mouse and chicken embryos by HCR (Fig. 2c-f), using the onset of gastrulation as time 0, and the time to reach half-maximum as a reference for the timing of gene expression. We found that Hoxb9, Pitx1, and Isl1 activation times were similar in both species: in the chick, where the forelimb and hindlimb initiate at nearly the same time, expression of Tbx5, Tbx4, Pitx1 and Isl1 are all initiated simultaneously. Conversely in the mouse, where hindlimb initiation is delayed relative to the forelimb, Hoxb9, Pitx1 and Isl1 are still activated together with Tbx5 despite the delay of Tbx4

(Fig. S2d-e; Fig. 2d,f). These data suggest that the delay in Tbx4 expression in the mouse embryo (22-hours after Hoxb9/Isl1/Pitx1 in mouse vs 2-hours in chicken) is not a consequence of delayed specification of the hindlimb lateral plate mesoderm (LPM), or a lag in the expression of known upstream activators.

Shifted timing of Tbx4 activation is not due to alterations in associated cis-regulatory elements

Heterochrony is an important mode of evolutionary change. The modern model posits that evolutionary change is largely attributable to mutations in cis-regulatory elements (CREs) (*31*). To determine whether CREs changes proximal to Tbx4 are responsible for the shifted timing of that gene's expression in the mouse, we sought to compare Tbx4 enhancer activity between mouse and chicken. For the mouse embryo, previous studies identified two genomic regions, named HLEA and HLEB, as necessary and sufficient to activate Tbx4 expression in the developing hindlimb (*32*). To identify chicken Tbx4 enhancers, we took advantage of an ATAC-seq analysis previously carried out in the lab (*33*), and selected regions that showed accessibility in HH18 hindlimb mesenchyme but not in the forelimb or flank. This criterion filtered the pool into 4 candidate genomic regions located within 100kb of Tbx4 transcriptional start site (Fig. 3a, Fig. S3a). To test whether these regions can drive the transcription in a pattern resembling that of endogenous Tbx4, we electroporated enhancer:Citrine reporter constructs, each carrying a candidate region, into chicken forelimb, flank or hindlimb tissues at HH14 (Fig. 3b). When the electroporated embryos were examined at HH18, 1 of the 4 candidate regions drove strong and restricted signal to the hindlimb tissue (Fig. 3c-d; Fig. S3a). This enhancer was designated as Tbx4-Rec1. To reveal the temporal activation pattern of Tbx4-Rec1, we quantified Citrine signal in hindlimb tissues of different stages by flow cytometry. This revealed that Tbx4-Rec1 activity is initiated at HH12 and becomes strong by HH16, paralleling the timing of endogenous Tbx4

expression (Fig. 3e). Thus, Tbx4-Rec1 activity resembles the expression profile of Tbx4 both spatially and temporally in the chicken embryo (Fig. 1c-d). Finally, to determine whether Tbx4-Rec1 is functionally required for Tbx4 expression, we inhibited the endogenous Tbx4-Rec1 region by deploying the dCas9-KRAB assay, which utilizes a catalytically dead Cas9 fused to the Krüppel-associated box (KRAB) transcriptional repression domain. This system, guided by specifically designed gRNAs targeting Tbx4-Rec1, acts to methylate the genomic region, thereby repressing it (*34*). We electroporated a construct carrying a gRNA targeting the middle position of Tbx4-Rec1 and the coding sequence of dCas9-krab, into the HH12 hindlimb field of chicken embryos. After 12 hours, the electroporated cells showed significant reduction of Tbx4 transcripts when compared to non-electroporated counterparts, or cells electroporated with a control gRNA (Fig. 3f-g). Together, these experiments implicate Tbx4-Rec1 as a critical enhancer for Tbx4 expression in the embryonic chicken hindlimb.

Sequence analyses suggest that the 3' DNA sequence of Tbx4-Rec1 highly resembles that of the mouse Tbx4 enhancer, HLEB (Fig. S3b). This suggests that the chicken Tbx4-Rec1 and mouse HBEB Tbx4 enhancers are homologous sequences. There is no obvious counterpart to HLEA in the chick genomic sequence near the Tbx4 gene(*32*). To test whether the mouse and chick enhancers are functionally conserved, we performed enhancer-swap experiments to orthogonally express the Tbx4 enhancers across species. To introduce the mouse Tbx4 enhancer into the chicken embryo, we performed electroporation experiments with Citrine reporter constructs carrying either HLEA or HLEB, as above (Fig. 3d-e). We found that both HLEA and HLEB were strongly activated, driving reporter expression at a similar level to Tbx4-Rec1(Fig.3d). Moreover, the timing of activation of both mouse enhancers was similar to that of Tbx4-Rec1 (Fig. 3e, Fig. 1d). To introduce the chicken Tbx4 enhancer into the mouse embryo, we produced Embryonic Stem cells (ES)-embryo chimeras (Fig. 3h). We first generated transgenic mouse ES cell lines each with a random genomic insertion of a Tbx4-Rec1:Citrine reporter cassette (Fig. 3h). The

transgenic ES cells were then aggregated to 8-cell stage mouse embryos, which were transferred to pseudo-pregnant female mice, and recovered at stages before and after Tbx4 expression. We optimized the ES cells aggregation protocol to achieve nearly full donor chimerism (Fig. S3c, *Methods*). We first examined HLEB:Citrine activity as positive control. As expected, no Citrine signal can be detected in the hindlimb LPM region from embryos recovered at E8.75 (Fig. S3c); However, strong activity can be detected only in hindlimb but not forelimb regions at E9.75 (Fig. S3d). Such an activation pattern recapitulates the endogenous mouse Tbx4 expression. We then examined Tbx4-Rec1:Citrine activity, and found that, similar to HLEB:Citrine, no Citrine signal was seen at E8.5, but strong activation was detected at E10.0 in the hindlimb (Fig. 3h). The inter-species enhancer analyses thus demonstrate that the mouse and chicken Tbx4 enhancers are functionally equivalent, and that any sequence variation between them are insufficient to account for the temporal shift in Tbx4 expression observed in the mouse embryo.

NFKB transcription factors are negative regulators of Tbx4 expression

Having ruled out the contribution of cis-regulatory elements to the delayed expression of Tbx4 in the mouse, we turned into the alternative model that differentially expressed trans-acting factors are responsible for difference in the timing of Tbx4 expression between the two species. To address this hypothesis, we conducted bulk RNA-sequencing of forelimb and hindlimb tissues from E8.5 and E9.75 mouse embryos, as well as forelimb and hindlimb tissues of HH12 chicken embryos (Fig. S4a).

Consistent with literature, our sequencing analyses identified Tbx5 and Raldh1a2 as significantly enriched in forelimb tissues(*12, 35*), and Cdx2, Evx1, Pitx1 as enriched in the hindlimb tissues across both species(*25, 36, 37*) (Fig. S4a). Comparing between stages, we found about 200 genes differentially expressed between E8.5 and E9.75 hindlimb tissues in the mouse.

To identify differentially expressed genes that might be functionally important for Tbx4 expression, we reviewed the documented function of each gene, and filtered out those with known discordant expression in HH12 chicken hindlimb, narrowing the focus to 22 factors related to metabolism, paracrine signaling, and transcription regulation (Table S1). To test whether the expression of any of these factors impact Tbx4 expression, we mis-expressed each gene in the chicken hindlimb. We designed two types of assays based on the gene's expression profile: 1) potential inhibitors: genes with higher expression at E8.5 than E9.5 were overexpressed in the HH12 chicken hindlimb field, and their impact on Tbx4 expression assessed at HH23. 2) potential activators: genes upregulated from E8.5 to E9.75 were overexpressed in gastrulating HH4 chicken embryos to evaluate potential advancement in Tbx4 expression by HH10.

This screen identified cRel as a potent repressor of Tbx4 expression (Fig. 4d-f; Fig. S4b-c). cRel is an effector of the NFKB signaling pathway involved in immune and stress response. We find that overexpression of cRel results in a marked reduction in hindlimb bud size and consistently lower Tbx4 transcript levels only in electroporated cells, suggesting a cell-autonomous effect of cRel in blocking Tbx4 expression (Fig. 4d; Fig. S4b-c).

Analysis of cRel knockout mouse embryos from E8.5 to E9.5 revealed that cRel-null embryos exhibited significant elevation of Tbx4 expression in hindlimb tissues at E8.5 compared to heterozygous littermates (Fig. 4e-f). However, this ectopic expression of Tbx4 was not observed across all cells, and predominantly occurred on only one side of the embryo (Fig. 4e). Despite this heterogeneous expression, the increased Tbx4 levels were sufficient to advance EMT timing by E9.0, as cRel null hindlimb tissues show a significant higher proportion of mesenchymal cells than heterozygous at E9.0 (Fig. 4g-h). Possibility due to the partial penetration, we found no difference in hindlimb bud size between cRel null and heterozygous littermates at E9.5 (Fig. S4d-e).

One possible explanation for the partial penetrance we observed could be redundancy with related factors co-expressed in the limb bud. Besides cRel, the NFKB family includes 4 other transcription factors, RelA, RelB, NFKB1 and NFKB2. Of the 5 factors, cRel, RelA and NFKB1 were detectable in mouse E8.5 hindlimb tissues in bulk RNA-seq (Fig. S4b). To understand whether other NFKB transcription factors similarly inhibit Tbx4 expression, we overexpressed RelA or NFKB1 in chicken hindlimb. We found that the overexpression of RelA, but not NFKB1, led to significant reduction of hindlimb bud size (Fig.4d). Examination of Tbx4 expression revealed a significant downregulation of Tbx4 transcripts in cells overexpressing RelA. By analyzing a recently published single-cell RNA sequencing data set, we found that the expression dynamics of cRel and RelA were similarly downregulated from E8.5 to E9.5 in the LPM(*38*). These data suggest RelA as a potential compensatory factor that may delay Tbx4 expression akin to cRel.

Altogether, the top-down approach using RNA-sequencing analyses reveals a previously unreported inhibitory role of NFKB transcription factors in delaying Tbx4 expression in the developing mouse hindlimb bud.

Maternal hypoxia impedes Tbx4 expression in the hindlimb

Building on our findings that the downregulation of cRel and RelA from pre- to post-hindlimb initiation stages may be responsible for the delayed activation of Tbx4 in mice, we next sought to elucidate the regulatory mechanisms governing their temporal expression. We were intrigued, in this regard, by the recent finding that mouse embryonic stem cells differentiated *in vitro* into hindlimb bud progenitors initially expressing Tbx5 and Tbx4, although these cells ultimately default to a hindlimb bud fate and express hindlimb markers,Tbx4(*20*). This suggested that a difference between *in vitro* culture and *in utero* conditions impact the timing of Tbx4 expression. One parameter that caught our attention as potentially being different in the two settings was the

level of oxygen present. Hypoxia can induce the expression of NFKB transcription factors in a number of contexts(*39, 40*), and importantly, evidence suggest that chicken eggs develop in environment close to normoxia (20%) whereas early mouse embryos are in hypoxia (2%-5%)(*41-43*). Importantly, there is a transition in the mouse embryo from low oxygen levels to normoxia as the placental connection to the maternal circulation becomes robust, at a time correlating with hindlimb initiation. Correspondingly, while chicken embryos exhibit low levels of nuclear Hif1a in the hindlimb field at HH12, mouse embryos at the comparable stage, E8.5, showed high levels of nuclear Hif1a. The nuclear Hif1a is diminished one day later, at E9.5, coinciding with robust Tbx4 expression and hindlimb EMT initiation (Fig. 5a-c).

To test whether oxygen levels could play a role in regulating the timing of Tbx4 expression in mouse embryos, we optimized an *ex-utero* culture system that allowed gastrulating embryos, dissected at E6.5, to develop until approximately E8.75 (Fig. 5d; Fig. S5a; *Methods*). The culture method is based on previous protocols(*42, 44*) but with two modifications: 1) 5% FBS was added into the culture medium as an alternative to human cord serum; 2) the ecto-placental cone (EPC) was removed to enhance oxygen equilibration within and surrounding the embryonic tissues. The latter modification was based on the observation that in the presence of an intact EPC, Hif1a expression was not completely extinguished in embryos cultured in normoxia conditions (Fig. S5b), likely due to inefficient gas penetration of the yolk sac layer. The cultured embryos generally attain a similar morphology to naturally developed E8.5 embryos in the formation of head-fold, allantois, and a clear distinction of anterior and posterior regions. There were occasional defects in the epithelization of somite tissues, which is likely due to the lack of sufficient mechanical cues in culture(*45*). Nonetheless, we found robust expression of forelimb field and hindlimb field markers Tbx5 and Pitx1, indicating normal differentiation of LPM lineages (Fig. 5e).

Leveraging the *ex-utero* culture system, we compared gene expression under different oxygen conditions. We recovered embryos at E6.75, and cultured them for 1.5 days, in either 5% or 20%

oxygen, which correspond to normoxia and hypoxia conditions. Remarkably, we found consistent activation of Tbx4 transcripts in mouse embryos cultured in normoxia condition, which did not occur in those cultured in hypoxia condition (Fig. 5e,g). Moreover, this activation of Tbx4 in normoxia-grown embryos is more pronounced than seen in cRel knockout embryos. Nearly all these embryos showed premature, elevated, bilateral expression of Tbx4 (Fig. 5e-g). The normoxia cultured embryos additionally show significant upregulation of Pitx1 in the posterior LPM, although the phenotype was less strong (Fig. S5c). This effect was specific to these hind limb genes as, in contrast, the normoxia cultured embryos showed no significant change in Tbx5 expression (if anything, there was a trend towards down-regulation) (Fig. 5f). Together, these results suggest that forced elevation of oxygen levels induce a precocious onset of hindlimb induction including Tbx4 expression and EMT, in mouse embryos. We could not carry out the reciprocal experiment, and ask whether culture in hypoxia delays hindlimb initiation in avian embryos because early chick embryos fail to develop under hypoxia condition.

We then asked whether the precocious expression of Tbx4 in normoxia-cultured mouse embryos would lead to an acceleration of limb bud initiation. To that end, we examined the status of EMT in normoxia-cultured embryos after 48 hours, the equivalent of E8.75. Using F-actin and laminin polarization as markers, we found that hindlimb embryos cultured in normoxia condition show a significantly higher proportion of mesenchymal cells in the hindlimb field (Fig. 5h-i). Moreover, we found a correlation between Tbx4 expression and the EMT status, such that regions with higher Tbx4 expression display more multi-layered mesenchymal cells (Fig. S5d). Together these results suggest that higher oxygen levels accelerate hindlimb development, and support a model where maternal hypoxic conditions in the early developing mouse embryo act to specifically delay hindlimb development.

Finally, to confirm that hypoxic conditions modulate the timing of Tbx4 activation by regulating NFKB transcription, we performed qPCR on dissected hindlimb field tissues from embryos

cultured under normoxia or hypoxia conditions. Consistent with the RNA-sequencing analyses, among the NFKB family members, only the transcripts of RelA, cRel and NFKB1 can be readily amplified (Fig.5j, Fig. S4b). Moreover, we found that the hindlimb tissues cultured in hypoxic conditions showed significant elevation of cRel, although non-significant expressional change of RelA and NFKB1 relative to the normoxia condition (Fig. 5j; Fig.S5e-f). These findings substantiate the hypothesis that transitioning from hypoxia to normoxia triggers the downregulation of cRel, thereby activating Tbx4 expression, and hence modulating the timing of limb development in mouse embryos.

Discussion

Despite growing interest in the study of developmental timing[43-45], mechanistic understanding of heterochronic change remains limited. Our study suggests a model explaining the observed heterochronic delay (post-displacement) in the onset of hindlimb formation in mammalian embryos relative to birds by hypoxia (Fig. 6). Avian species primarily obtain oxygen through a gas chamber and passive transport through the eggshell, which are limited in their oxygen-carrying capacity. As such, embryonic tissues gradually become hypoxic as cell numbers and tissue size increase(*41*). In contrast, mammals initially develop under hypoxic conditions due to the inaccessibility of embryonic tissues to oxygen. Subsequently, the maturation of placental functions allows efficient maternal-fetus oxygen exchange through allantois and blood circulation, and thus allows the transition to normoxia around mid-gestation stage[36-38]. Mammalian embryos have evolved to exploit this increase in available oxygen as a cue to alter the timing of hindlimb formation relative to that seen in bird embryos. In particular, in the chick embryo Pitx1 and Isl1 activate Tbx4 expression within 2-hours of their expression. But in the mouse embryo, Tbx4 (but not its functional forelimb equivalent Tbx5) has been brought under the repressive influence of the NFKB family members cRel and RelA, which have been co-opted for this purpose by being

up-regulated under hypoxic conditions. As a consequence, although expression of Pitx1 and Isl1 is activated in the hindlimb field at an equivalent developmental time as observed in the chick, they are unable to induce Tbx4 expression for 18-22 hours, until oxygen levels rise and hence NFKB activity is diminished.

Our results show that that limb heterochrony in mammals starts at the very first step of limb development, when Tbx4 induces EMT. This contrasts with the delay in forelimb (wing) development in emu embryos, in which the reduced forelimb growth rate relates not to the limb initiation, but rather to changes in post-initiation cell proliferation(*33*). In this case, Tbx5 expression occurs on time, but the expression of Fgf10, a key regulator of limb progenitor proliferation is reduced. This distinct mechanism is required in emus since their embryos, like chicks, lack an early hypoxic phase, and highlights the diverse levels of the limb developmental program that can be exploited by evolution to alter the tempo of limb outgrowth.

The delay in hindlimb development is even more pronounced in marsupial embryos, where it persists for longer period of time compared to placental mammals. As a result, the precocially born fetus displays an anatomically matured forelimb, capable of functioning in climbing to the pouch, but a still underdeveloped hindlimb(*3*). Both forelimb acceleration and hindlimb delay have been posited as being responsible for limb heterochrony in marsupials(*46-48*). Indeed, multiple mechanisms, involving a number of different levels of the limb morphogenesis program, may be involved in regulating this more extreme case of limb heterochrony. In this context, it is worth noting that, in spite of being much more extreme at later stages, the severity of marsupial limb heterochrony is similar to that of the mouse embryo at the limb initiation stage (*49*). Moreover, in the grey short-tailed opossum (*Monodelphis domestica*), both Tbx5 in the forelimb and Pitx1 in the hindlimb are detectable at least half a day earlier than Tbx4 (*46*), as is the case in mice. These results at least raise the possibility that the mechanism we identify here as underlying eutherian hindlimb heterochrony may also be utilized in marsupial embryos as one of the adaptive changes

contributing to their more severe hindlimb developmental delay. If so, then limb heterochrony in placental mammals might be an evolutionary vestige from the non-placental common ancestor of both marsupials and eutherian mammals, rather than having arisen *de novo* within the placental stem lineage.

One of the most intriguing findings of our study is the role of hypoxia in regulating the timing of hindlimb initiation. The transition from oviparity to viviparity dramatically alters the developmental environment from avian to mammalian species, with significant differences in oxygen levels as well as altering the level of accessibility of nutrients during the early embryonic development. As both parameters increase by placenta maturation, the level of oxygen can be viewed as a sensor of the level of nutrient availability. Mammalian embryos evolved to take advantage of this sensor to control the timing of development of less immediately required structures in an “energy trade-off strategy” to cope with limited nutrient availability.

When ectopically expressed, both cRel and RelA blocked the expression of Tbx4 and consequently the hindlimb bud formation. It is known that cRel can competitively block the binding of RelA to the chromatin in other contexts (*50*). Therefore, although hypoxia does not significantly alter the expression of RelA, it is likely that RelA compensates for cRel activity only when cRel is depleted, explaining the weaker phenotype seen in cRel mutant embryos comparing to hypoxia condition.

Besides the activation of NFKB transcription factors described here, hypoxia can influence the activities of multiple pathways including protein synthesis rate, oxidative phosphorylation levels, and mitochondrial biosynthesis—factors known to regulate developmental timing in various contexts. Conversely, it is noteworthy that the NFKB pathway activities can also mediate cellular metabolism in other systems.

Overall, our studies provide the first investigation of the molecular mechanisms regulating the limb heterochrony, an important embryonic adaptation to the *in utero* mammalian development. The mechanism we elucidate represents a novel use of hypoxia as a trigger for temporal events in the embryo. In a broader sense, this provides new insight into how the maternal environment regulates developmental timing.

References

1. M. K. Richardson *et al.*, Heterochrony in limb evolution: developmental mechanisms and natural selection. *J Exp Zool B Mol Dev Evol* **312**, 639-664 (2009).
2. V. Weisbecker, A. Goswami, S. Wroe, M. R. Sanchez-Villagra, Ossification heterochrony in the therian postcranial skeleton and the marsupial-placental dichotomy. *Evolution* **62**, 2027-2041 (2008).
3. A. L. Keyte, K. K. Smith, Heterochrony and developmental timing mechanisms: changing ontogenies in evolution. *Semin Cell Dev Biol* **34**, 99-107 (2014).
4. J. Gros, C. J. Tabin, Vertebrate limb bud formation is initiated by localized epithelial-to-mesenchymal transition. *Science* **343**, 1253-1256 (2014).
5. K. Sekine *et al.*, Fgf10 is essential for limb and lung formation. *Nat Genet* **21**, 138-141 (1999).
6. J. K. Takeuchi *et al.*, Tbx5 and Tbx4 trigger limb initiation through activation of the Wnt/Fgf signaling cascade. *Development* **130**, 2729-2739 (2003).
7. J. R. Barrow *et al.*, Ectodermal Wnt3/beta-catenin signaling is required for the establishment and maintenance of the apical ectodermal ridge. *Genes Dev* **17**, 394-409 (2003).
8. C. Rallis *et al.*, Tbx5 is required for forelimb bud formation and continued outgrowth. *Development* **130**, 2741-2751 (2003).
9. L. A. Naiche, V. E. Papaioannou, Loss of Tbx4 blocks hindlimb development and affects vascularization and fusion of the allantois. *Development* **130**, 2681-2693 (2003).
10. Y. Kawakami *et al.*, WNT signals control FGF-dependent limb initiation and AER induction in the chick embryo. *Cell* **104**, 891-900 (2001).
11. H. M. T. Choi *et al.*, Third-generation in situ hybridization chain reaction: multiplexed, quantitative, sensitive, versatile, robust. *Development* **145**, (2018).
12. J. K. Takeuchi *et al.*, Tbx5 and Tbx4 genes determine the wing/leg identity of limb buds. *Nature* **398**, 810-814 (1999).
13. H. Ohuchi *et al.*, The mesenchymal factor, FGF10, initiates and maintains the outgrowth of the chick limb bud through interaction with FGF8, an apical ectodermal factor. *Development* **124**, 2235-2244 (1997).
14. J. K. Ng *et al.*, The limb identity gene Tbx5 promotes limb initiation by interacting with Wnt2b and Fgf10. *Development* **129**, 5161-5170 (2002).
15. C. Rodriguez-Esteban *et al.*, The T-box genes Tbx4 and Tbx5 regulate limb outgrowth and identity. *Nature* **398**, 814-818 (1999).

16. D. Duboule, Temporal colinearity and the phylotypic progression: a basis for the stability of a vertebrate Bauplan and the evolution of morphologies through heterochrony. *Dev Suppl*, 135-142 (1994).
17. C. Minguillon *et al.*, Hox genes regulate the onset of Tbx5 expression in the forelimb. *Development* **139**, 3180-3188 (2012).
18. C. Moreau *et al.*, Timed Collinear Activation of Hox Genes during Gastrulation Controls the Avian Forelimb Position. *Curr Biol* **29**, 35-50 e34 (2019).
19. M. Tanaka *et al.*, BMP inhibition stimulates WNT-dependent generation of chondrogenic mesoderm from embryonic stem cells. *Stem Cell Res* **3**, 126-141 (2009).
20. S. Mori *et al.*, Self-organized formation of developing appendages from murine pluripotent stem cells. *Nat Commun* **10**, 3802 (2019).
21. M. Logan, C. J. Tabin, Role of Pitx1 upstream of Tbx4 in specification of hindlimb identity. *Science* **283**, 1736-1739 (1999).
22. V. Duboc, M. P. Logan, Pitx1 is necessary for normal initiation of hindlimb outgrowth through regulation of Tbx4 expression and shapes hindlimb morphologies via targeted growth control. *Development* **138**, 5301-5309 (2011).
23. J. Itou *et al.*, Islet1 regulates establishment of the posterior hindlimb field upstream of the Hand2-Shh morphoregulatory gene network in mouse embryos. *Development* **139**, 1620-1629 (2012).
24. V. Duboc *et al.*, Tbx4 function during hindlimb development reveals a mechanism that explains the origins of proximal limb defects. *Development* **148**, (2021).
25. D. P. Szeto *et al.*, Role of the Bicoid-related homeodomain factor Pitx1 in specifying hindlimb morphogenesis and pituitary development. *Genes Dev* **13**, 484-494 (1999).
26. G. Narkis *et al.*, Isl1 and Ldb co-regulators of transcription are essential early determinants of mouse limb development. *Dev Dyn* **241**, 787-791 (2012).
27. A. Ferrer-Vaquer *et al.*, A sensitive and bright single-cell resolution live imaging reporter of Wnt/ss-catenin signaling in the mouse. *BMC Dev Biol* **10**, 121 (2010).
28. T. Takemoto *et al.*, R26-WntVis reporter mice showing graded response to Wnt signal levels. *Genes Cells* **21**, 661-669 (2016).
29. A. Molotkov, N. Molotkova, G. Duester, Retinoic acid generated by Raldh2 in mesoderm is required for mouse dorsal endodermal pancreas development. *Dev Dyn* **232**, 950-957 (2005).
30. T. J. Cunningham *et al.*, Antagonism between retinoic acid and fibroblast growth factor signaling during limb development. *Cell Rep* **3**, 1503-1511 (2013).
31. S. Jeong *et al.*, The evolution of gene regulation underlies a morphological difference between two Drosophila sister species. *Cell* **132**, 783-793 (2008).
32. D. B. Menke, C. Guenther, D. M. Kingsley, Dual hindlimb control elements in the Tbx4 gene and region-specific control of bone size in vertebrate limbs. *Development* **135**, 2543-2553 (2008).
33. J. J. Young, P. Grayson, S. V. Edwards, C. J. Tabin, Attenuated Fgf Signaling Underlies the Forelimb Heterochrony in the Emu Dromaius novaehollandiae. *Curr Biol* **29**, 3681-3691 e3685 (2019).
34. N. Alerasool, D. Segal, H. Lee, M. Taipale, An efficient KRAB domain for CRISPRi applications in human cells. *Nat Methods* **17**, 1093-1096 (2020).
35. F. A. Mic, R. J. Haselbeck, A. E. Cuenca, G. Duester, Novel retinoic acid generating activities in the neural tube and heart identified by conditional rescue of Raldh2 null mutant mice. *Development* **129**, 2271-2282 (2002).
36. J. G. Savory *et al.*, Cdx2 regulation of posterior development through non-Hox targets. *Development* **136**, 4099-4110 (2009).
37. C. C. Bell *et al.*, The Evx1/Evx1as gene locus regulates anterior-posterior patterning during gastrulation. *Sci Rep* **6**, 26657 (2016).

38. C. Qiu *et al.*, A single-cell time-lapse of mouse prenatal development from gastrula to birth. *Nature* **626**, 1084-1093 (2024).
39. K. Yin, B. H. Juurlink, Regulation of expression of nuclear factor kappa B RelA in oligodendrocytes: effect of hypoxia. *Neuroreport* **11**, 1877-1881 (2000).
40. Y. Jiang *et al.*, Temporal regulation of HIF-1 and NF-kappaB in hypoxic hepatocarcinoma cells. *Oncotarget* **6**, 9409-9419 (2015).
41. C. Carroll *et al.*, Hypoxia Generated by Avian Embryo Growth Induces the HIF-α Response and Critical Vascularization. *Frontiers in Ecology and Evolution* **9**, (2021).
42. A. Aguilera-Castrejon *et al.*, Ex utero mouse embryogenesis from pre-gastrulation to late organogenesis. *Nature* **593**, 119-124 (2021).
43. D. Sakai *et al.*, Glycolytic activity is required for the onset of neural plate folding during neural tube closure in mouse embryos. *Frontiers in Cell and Developmental Biology* **11**, (2023).
44. L. H. Culshaw, D. Savery, N. D. E. Greene, A. J. Copp, Mouse whole embryo culture: Evaluating the requirement for rat serum as culture medium. *Birth Defects Res* **111**, 1165-1177 (2019).
45. M. Linde-Medina, T. H. Smit, Molecular and Mechanical Cues for Somite Periodicity. *Front Cell Dev Biol* **9**, 753446 (2021).
46. A. L. Keyte, K. K. Smith, Developmental origins of precocial forelimbs in marsupial neonates. *Development* **137**, 4283-4294 (2010).
47. L. B. Harrison, H. C. Larsson, Estimating evolution of temporal sequence changes: a practical approach to inferring ancestral developmental sequences and sequence heterochrony. *Syst Biol* **57**, 378-387 (2008).
48. A. Lyne, Observations on the breeding and growth of the marsupial Perameles nasuta Geoffroy, with notes on other bandicoots. *Australian Journal of Zoology* **12**, 322-339 (1964).
49. K. Y. Chew, G. Shaw, H. Yu, A. J. Pask, M. B. Renfree, Heterochrony in the regulation of the developing marsupial limb. *Dev Dyn* **243**, 324-338 (2014).
50. T. J. de Jesus, P. Ramakrishnan, NF-kappaB c-Rel Dictates the Inflammatory Threshold by Acting as a Transcriptional Repressor. *iScience* **23**, 100876 (2020).

Acknowledgment

We thank all members in Cepko-Tabin labs and Susan Dymecki lab, and Dr. Emma Farley, Dr. Scott Edwards for giving constructive comments on the project. We thank Dr. Macolm Logan and Dr. Ben Steventon for helpful discussions at the initial phase of the project. We also thank Dr. Nandan Nerukar and Dr. Marianne Bronner for the training of early chick culture experiments, Dr. Lina Du from mouse engineering core at Dana-farber with the help of embryo transfer, and Micron imaging core especially Dr. Paula Montero Llopis for imaging assistance.

Funding: Work on this topic is supported by a grant from the NIH, HD032443 to C.J.T, and a Human Frontier Science program long-term post-doctoral fellowship LT000676/2020-L to M.Z.

Author contribution: Conceptualization: M.Z; Formal analysis: M.Z, R.C.P. Funding acquisition: C.T.J, M.Z; Investigation: M.Z, C.L, C.T.J; Methodology: M.Z, C.T.J; Visualization: M.Z; Supervision: C.T.J; Writing-original draft: M.Z, C.T.J; Writing-review & editing: M.Z, R.C.P, C.L, C.T.J.

Competing interest: The authors declare no competing interests.

Data and materials availability: The bulk RNA-sequencing data will be deposited to NCBI GEO database. All other raw data are available upon reasonable request to the corresponding author.

List of Supplementary Materials

Materials and Method

Figs. S1-S5

Tables S1-S2

References 51-53

Figure legends

Fig.1. The expression of Tbx5 and Tbx4 correlate with the timing of Epithelial-to-mesenchymal transition (EMT) and the limb heterochrony. (**a**) Representative images of E9.5 and E9.75 mouse embryos sectioned at the hindlimb field to stain the F-actin and Laminin DAPI to reveal the epithelial/mesenchymal state of the cells. While at E9.5 the cells remain epithelial shapes, at E9.75, the cell completely transited to mesenchymal state. N=4 embryos for E9.5; N=2 embryos for E9.75. N=2 experiments. (**b**) Timeline showing the timings of EMT in forelimb and hindlimb and in mouse and chicken embryos. (**c**) Representative images of chicken hindlimb sections at HH12 and HH14 revealing the transcripts levels of Tbx4 by Hybridization chain

reaction (HCR), and co-stained with DAPI. (**d**) Quantification of chicken Tbx5 and Tbx4 transcripts levels across HH8-HH18 stages in forelimb and hindlimb tissues. The stage information is converted to hours post gastrulation initiation at HH4. HH8=27.5h, HH10 =35.5h, HH12=47h, HH14=51.5h, HH16=53.5h and HH18=72h. Dotted lines indicated the EMT timings of forelimb and hindlimb respectively. N=2-6 embryos are used for each tissue and each stage. (**e**) Representative images of E9.0 and E9.75 mouse hindlimb sections revealing the transcripts levels of Tbx4 by Hybridization chain reaction (HCR), and co-stained with DAPI. (**f**) Quantification of mouse Tbx5 and Tbx4 transcripts levels across E7.5 to E10.0 stages in forelimb and hindlimb tissues. The stage information is converted to hours post gastrulation initiation at HH4. E7.5=36h, E7.75=42h, E8.0=48h, E8.5=60h, E8.5=72h, E9.0=84h, E9.5=90h, E9.75=96h and E10.0=102h. Dotted lines indicated the EMT timing of forelimb and hindlimb respectively. N=2-4 embryos are used for each tissue and each stage. N=2 experiments. (**g**) Images showing chicken hindlimb at HH15 to stain Tbx4 transcripts by HCR and F-actin and DAPI to correlate with cellular state. Epithelial cells have lower level of Tbx4 than mesenchymal cells. dotted lines indicate magnified areas. (**h-i**) Quantifications of levels of Tbx5 (**h**) and Tbx4 (**i**) in epithelial and mesenchymal cells of chicken forelimb and hindlimb tissues. Dotted lines indicate the transitioning stage when epithelial and mesenchymal cells both present in the same tissue. A clear correlation with the levels of Tbx5 and Tbx4 to epithelial/mesenchymal state can be detected. N=8 embryos, N=2 experiments. Scale bars for overview images, 150μm; scale bars for magnified images, 15μm.

Fig.2. Upstream activators of Tbx4 show concordant expression with Tbx5 between chicken and mouse embryo. (**a**) Representative images of phosphorylated Smad proteins (p-Smad) staining in hindlimb tissues of chicken embryos at HH9, HH12 and mouse embryos at E8.0 and E8.5. Dotted lines indicate the magnified region. (**b**) Quantifications of p-Smad nuclear levels in chicken and mouse hindlimb tissues as in **a**. No significant differences in the kinetics of p-Smad activation are observed between conditions. N=34 cells for HH9 and N=20 cells for HH12 chicken

hindlimb tissues. N=2 embryos for each stage. N=60 cells for E8.0 and N=171 cells for E8.5 for mouse embryos. N=2-3 embryos for each stage. N=2 experiments. (**c**) Representative images of PITX1, ISL1 and HOXB9 expression revealed by HCR and co-stained with DAPI in HH10 and HH12 chicken hindlimb field tissues. Pitx1 and Isl1 are robustly expressed from HH12 chicken embryo. Dotted lines indicate magnified regions. (**d**) Quantifications of chicken PITX1, ISL1 and HOXB9 transcripts levels by HCR across HH8-18 stages of hindlimb tissues as in **a**. 2-4 embryos for each stage quantified. N=2 experiments. (**e**) Representative images of Pitx1, Isl1 and Hoxb9 expression revealed by HCR and co-stained with DAPI in E8.5 and E9.5 mouse hindlimb field tissues. Pitx1 and Isl1 are robustly expressed from E8.5 in mouse embryo. Dotted lines indicate magnified regions. (**f**) Quantifications of mouse Pitx1, Isl1 and Hoxb9 transcripts levels by HCR across E7.5-E10.0 stages of hindlimb tissues as in **c**. 2-3 embryos for each stage, N=2 experiments. For **b** and **d**, data are shown as mean ± S.E.M. Data is shown as mean ± S.E.M. Scale bars for overview images, 150μm; scale bars for magnified images, 15μm.

Fig.3. cis-regulatory elements responsible for Tbx4 activation are conserved between chicken and mouse embryos. (**a**) Chromatin accessibility of genomic regions of chicken Tbx4 enhancer designated as Tbx4-Rec1. Data is extracted from ATAC-seq experiments in Young et al., 2019(*33*). Tbx4-Rec1 genomic region is higher accessible in hindlimb tissues than forelimb and flank tissues in HH18 chicken embryos. (**b**) Scheme of enhancer bashing assay. Enhancer:reporter constructs carrying each enhancer candidates for chicken Tbx4 expression were electroplated in HH12 chicken hindlimb fields. pCMV-mCherry construct is co-electroplated as electroporation control. The enhancer activity was examined at HH18 and HH23. (**c**) Quantification of the enhancer activity of the 4 chicken Tbx4 enhancer candidates at HH18 by flow cytometry. Enhancer activity is calculated as the signal ratio of Green channel/Red channel. Data is shown as mean value for each condition. N=10 embryos disassembled for each group, N=3 experiments. Only Tbx4-Rec1 show high activation. (**d**) Representative images of chicken

hindlimb tissues electroplated with Tbx4-Rec1:Citrine constructs and sectioned at HH18 and HH23 to examine the enhancer activity by Citrine and DAPI. (**e**) Quantifications of mouse and chicken Tbx4 enhancer activities by flow cytometry of chicken hindlimb cells electroplated by each of the enhancer. Data shown as mean± S.E.M N=30 embryos were disassembled for each condition in total, N=3 experiments. (**f**) Representative images of HH16 chicken hindlimb cells electroplated by dCas9-Krab constructs containing control gRNA or with gRNA targeting Tbx4-Rec1 for 13h, and fixed and visualized Tbx4 transcripts by HCR and co-stained with ZsGreen and DAPI. Yellow circles delineate electroplated cells. (**g**) Quantifications of Tbx4 transcripts in conditions shown in **f**. Tbx4 transcripts are significantly downregulated specifically in cells transfected with Tbx4-Rec1 gRNA. ****$p<0.0001$, ns, not significant, Mann-Whitney test. Data shown as individual points with mean± S.E.M. Each dot indicates one cell. N=19 cells for Ctrl gRNA Citrine-; N=38 cells for Ctrl gRNA Citrine+; N=30 cells for Tbx4-Rec1 gRNA Citrine-; N=16 cells for Tbx4-Rec1 gRNA Citrine+. N=2-3 embryos for each condition, N=2 experiments. (**h**) Scheme for the strategies for producing ES cell-embryo chimera. Wildtype ES cells were transfected with constructs containing piggybac transposase and piggybac LTRs enclosing enhancer:Citrine cassette and CMV:H2B-mCherry cassette. The transgenic ES cells were then aggregated with E2.5 (8-cell stage) mouse embryos and cultured until E3.5. The chimeric embryos were then transferred to pseudo-pregnant females and dissected at deserved stages before and after Tbx4 expression. The representative images of ES-embryo chimeric embryos carrying Tbx4-Rec1:Citrine transgenic ES cells recovered at E8.5 and E10.0 to reveal the enhancer activity by Citrine and mCherry, and co-visualized Tbx4 transcripts by HCR and DAPI. N=6 embryos. N=2 experiments. Scale bars for overview images, 150μm; scale bars for magnified images, 15μm.

Fig.4. Higher cRel expression represses Tbx4 expression in the hindlimb of mouse embryo. (**a**) Representative images of E8.75 and E9.75 mouse embryos visualizing cRel expression by

HCR (co-stained with DAPI) in forelimb and hindlimb tissues. N=2 embryos for each condition. N=2 experiments. (**b**-**c**) RNA-sequencing data (**b**) and HCR quantification (**c**) of cRel expression in E8.5 forelimb and hindlimb tissues and E9.75 hindlimb tissues. cRel expression is downregulated from E8.5 to E9.75 hindlimb tissue. For **b**, *$p<0.05$, Kruskal-Wallis test. N=10 embryos were pooled for each repeat, tissue and stage. N=4 repeats. For **c**, N=2 embryos for each condition. N=2 experiments. (**d**) Representative images of chicken embryos electroplated with ZsGreen only (as a control), cRel:ZsGreen or RelA:ZsGreen into HH13 hindlimb tissue of chicken embryos and cultured for 2 days (at HH23) to examine the hindlimb bud formation and Tbx4 expression by HCR (and co-stained with DAPI). cRel or RelA overexpression significantly reduced the hindlimb bud formation only in the electroplated side of the embryo, and resulted in significant downregulation of Tbx4 expression only in the electroporated cells. N=8 embryos for ZsGreen, N=13 embryos for cRel:ZsGreen, and N=6 embryos for RelA. N=3 experiments. Dotted lines indicate locations of the cross-sections. (**e**) Representative images of the posterior section of cRel heterozygous and homozygous knockout embryos dissected at E8.5, visualized Tbx4 by HCR, and co-stained with DAPI. Pitx1 transcripts were visualized by HCR to reveal the location of the hindlimb field region. Dotted lines indicate magnified regions. (**f**) Quantifications of Tbx4 transcripts in the hindlimb field of conditions shown in **e**. **$p<0.01$, Mann Whitney test. Each dot represents an embryo. Data is shown as mean ± S.E.M. N=7 experiments. (**g**) Representative images of cRel heterozygous and homozygous knockout embryos dissected at E9.0 and examined the epithelial or mesenchymal state of the hindlimb field cells by the immunostaining of F-actin, Laminin and DAPI. Dotted lines indicate magnified regions. (**h**) Quantifications of epithelial/mesenchymal cells in hindlimb tissues from conditions in **g**. ****$p<0.0001$, Fisher's exact test. Data is shown as bar chart, numbers in each bar represents the number of cells examined. N=7 embryos for cRel knockout, N=7 embryos for cRel heterozygous mutants. N=2 experiments. Scale bars for overview images, 150μm; scale bars for magnified images, 15μm.

Fig.5. Level of oxygens regulate the timing of Tbx4 expression partially through NFKB transcription factors' expression. (**a**-**b**) Representative images of Hif1a staining in forelimb and hindlimb tissues of HH12 chicken embryo (**a**) and E8.5 and E9.25 mouse embryos (**b**). Dotted lines indicate magnified regions. (**c**) Quantifications of the levels of nuclear Hif1a (normalized to DAPI) in conditions shown in a-b. ****$p<0.0001$, One way ANOVA test. Data shown as mean ± S.E.M, each dot indicates a cell. N=2 embryos for each stage. N=2 experiments. (**d**) Scheme of *ex-utero* culture system. E6.75 mouse embryos were recovered and the ecto-placental cone was removed, the embryos were then cultured in 5% or 20% O_2 for 1.5 days (36h), after which the embryos reach the stage the morphology of which assemblies that of E8.5 mouse embryo. (**e**) *Ex-utero* cultured embryos in 5% or 20% O_2 level as in (**d**) were fixed to examine transcripts levels of Tbx5, Pitx1 and Tbx4 (co-stained with DAPI) in forelimb and hindlimb regions after 1.5 days of culture. Natural E8.5 embryos were compared as control. Dotted lines indicate magnified regions. (**f**-**g**) Quantifications of Tbx5 (**f**) and Tbx4 (**g**) in forelimb and hindlimb tissues from conditions shown in **e**. ns, not significant, *$p<0.05$, ***$p<0.001$, ****$p<0.0001$, One way ANOVA test. Data shown as mean ± S.E.M. Each dot indicates an embryo. N=8 experiments for both 5% and 20% O_2. (**h**) Representative images of *ex-utero* cultured embryos in 5% and 20% O_2 for 2 days and immunostained with laminin, F-actin and DAPI for revealing epithelial/mesenchymal state of the hindlimb cells. (**i**) Quantification of number of epithelial and mesenchymal cells for conditions shown in **h**. ****$p<0.0001$, Fisher's exact test. Data is shown as bar chart, numbers in each bar represents the number of cells examined. N=4 embryos for 5% O_2; N=3 embryos for 20% O_2. N=2 experiments. Significant higher proportion mesenchymal cells are seen in hindlimb cells cultured in 20% O_2. (**j**) Quantitative PCR (qPCR) analysis of cRel, RelA, NFKB1 expression in embryos ex-utero cultured in 5% or 20% O_2. **$p<0.01$, ns, not significant. Mann-Whitney test. Data shown as mean ± S.E.M. Each data point represents one experiment. Hypoxia culture induces significant upregulation of cRel. Scale bars for overview images, 150μm; scale bars for magnified images, 15μm.

Fig.6. Summary model. Forelimb and hindlimb develop at different times from the limb initiation stage in the mouse embryo but much less so in the chicken, our results show that the limb initiation heterochrony in the mouse is mediated by the hypoxia environment that the mouse embryo exposes to in the limb field specification stage. The hypoxia environment inhibits limb initiation by delaying the hindlimb initiation factor such as Tbx4. Hypoxia's effect on tbx4 expression is at least partially mediated by NFKB transcription factors such as cRel. Altogether, our findings reveal the first example of the mechanisms behind limb initiation heterochrony and suggest a novel role of the maternal environment in directing the timing of embryonic development during post-implantation stages.

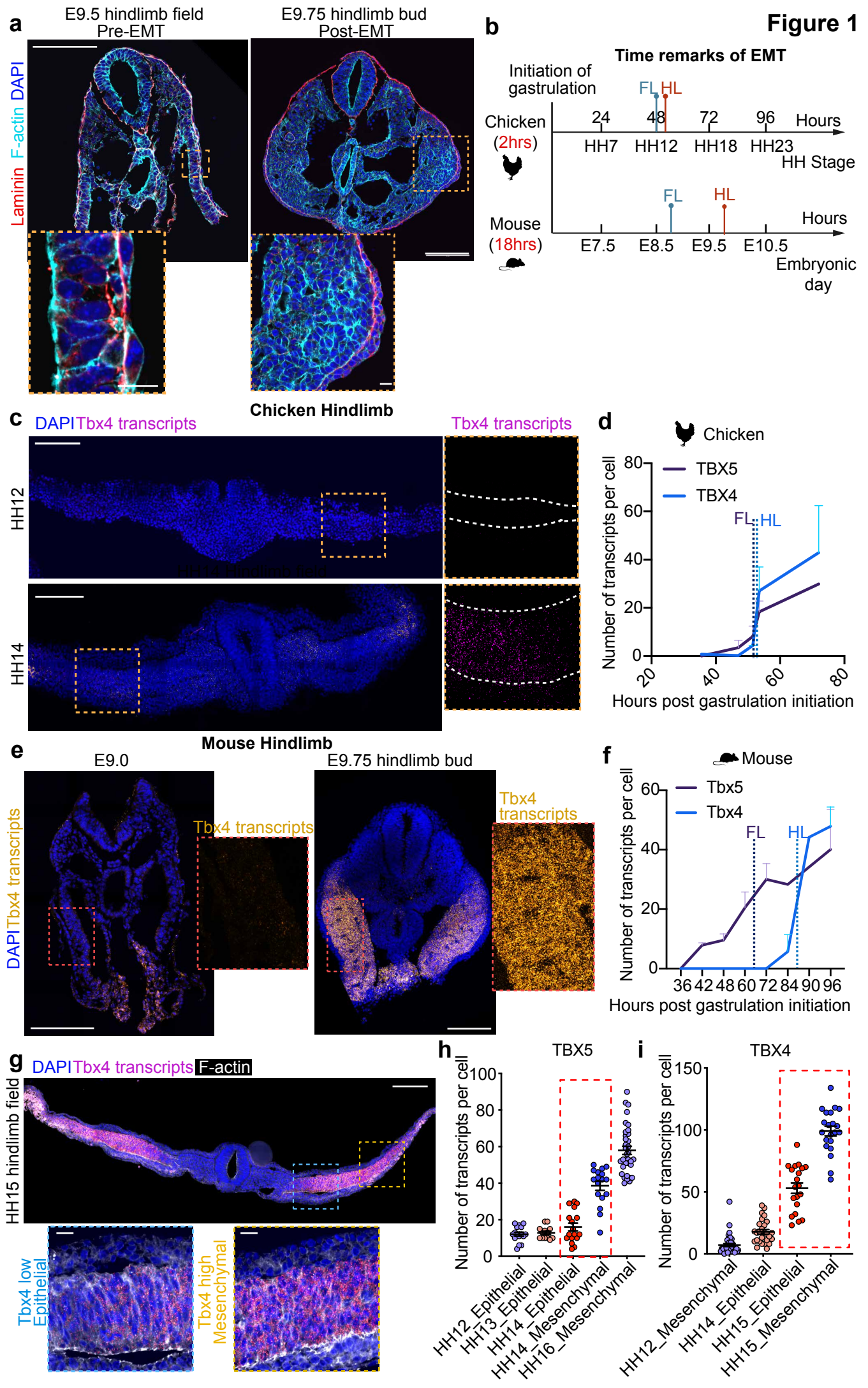
Figure 1
a
E9.5 hindlimb field
Pre-EMT
E9.75 hindlimb bud
Post-EMT
DAPI
F-actin
Laminin
b
Time remarks of EMT
Initiation of gastrulation
FL
HL
Chicken
(2hrs)
24
48
72
96
Hours
HH7
HH12
HH18
HH23
HH Stage
Mouse
(18hrs)
E7.5
E8.5
E9.5
E10.5
Embryonic day
c
Chicken Hindlimb
DAPI Tbx4 transcripts
Tbx4 transcripts
HH12
HH14
HH14 Hindlimb field
d
Chicken
TBX5
TBX4
Number of transcripts per cell
Hours post gastrulation initiation
e
Mouse Hindlimb
E9.0
E9.75 hindlimb bud
DAPI Tbx4 transcripts
Tbx4 transcripts
f
Mouse
Tbx5
Tbx4
Number of transcripts per cell
Hours post gastrulation initiation
g
DAPI Tbx4 transcripts F-actin
HH15 hindlimb field
Tbx4 low Epithelial
Tbx4 high Mesenchymal
h
TBX5
Number of transcripts per cell
HH12_Epithelial
HH13_Epithelial
HH14_Epithelial
HH14_Mesenchymal
HH16_Mesenchymal
i
TBX4
Number of transcripts per cell
HH12_Mesenchymal
HH14_Epithelial
HH15_Epithelial
HH15_Mesenchymal

Figure 2

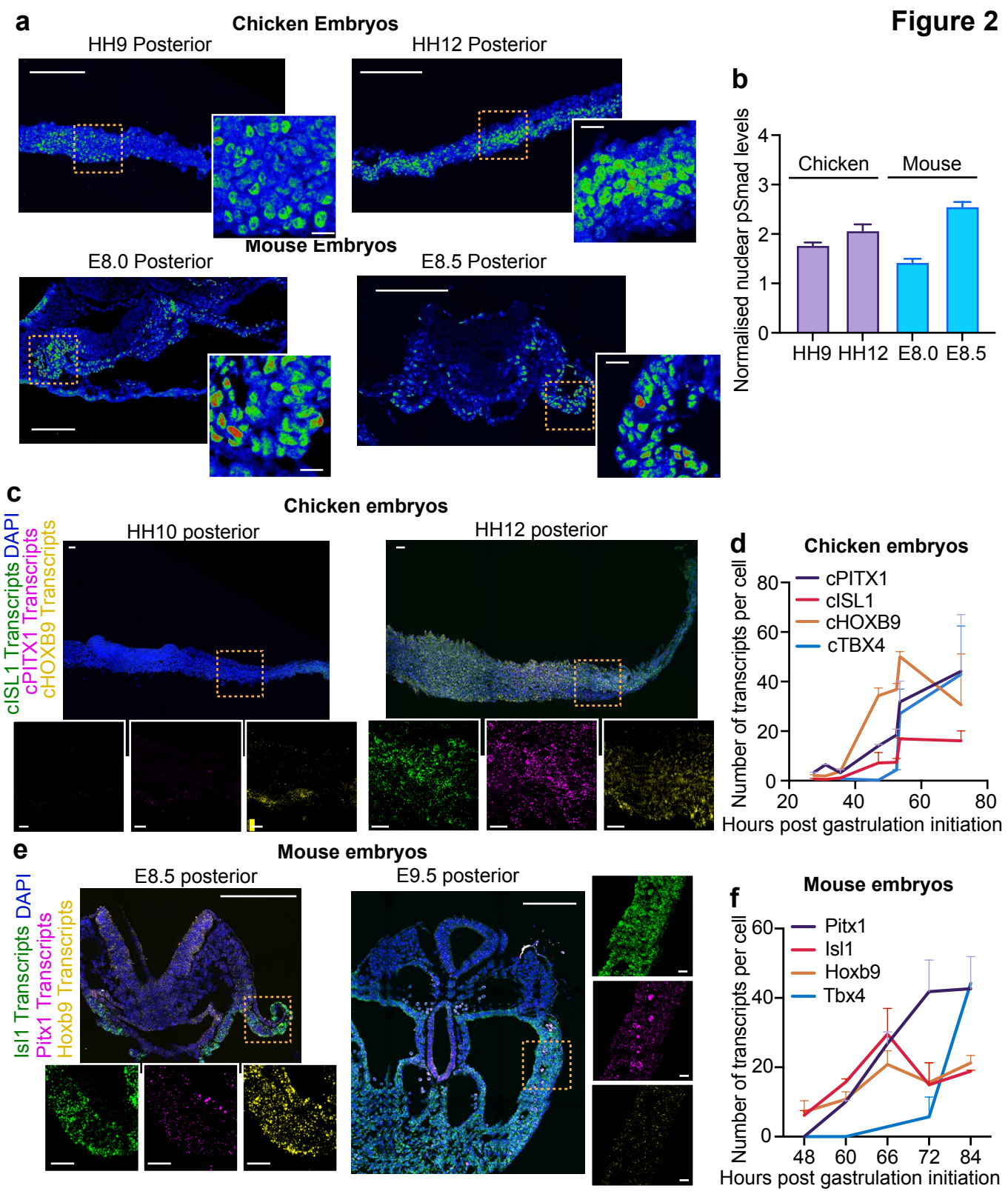
a
Chicken Embryos
HH9 Posterior
HH12 Posterior
Mouse Embryos
E8.0 Posterior
E8.5 Posterior
b
Normalised nuclear pSmad levels
Chicken
Mouse
HH9
HH12
E8.0
E8.5
c
Chicken embryos
HH10 posterior
HH12 posterior
cISL1 Transcripts DAPI
cPITX1 Transcripts
cHOXB9 Transcripts
d
Chicken embryos
Number of transcripts per cell
cPITX1
cISL1
cHOXB9
cTBX4
Hours post gastrulation initiation
e
Mouse embryos
E8.5 posterior
E9.5 posterior
Isl1 Transcripts DAPI
Pitx1 Transcripts
Hoxb9 Transcripts
f
Mouse embryos
Number of transcripts per cell
Pitx1
Isl1
Hoxb9
Tbx4
Hours post gastrulation initiation

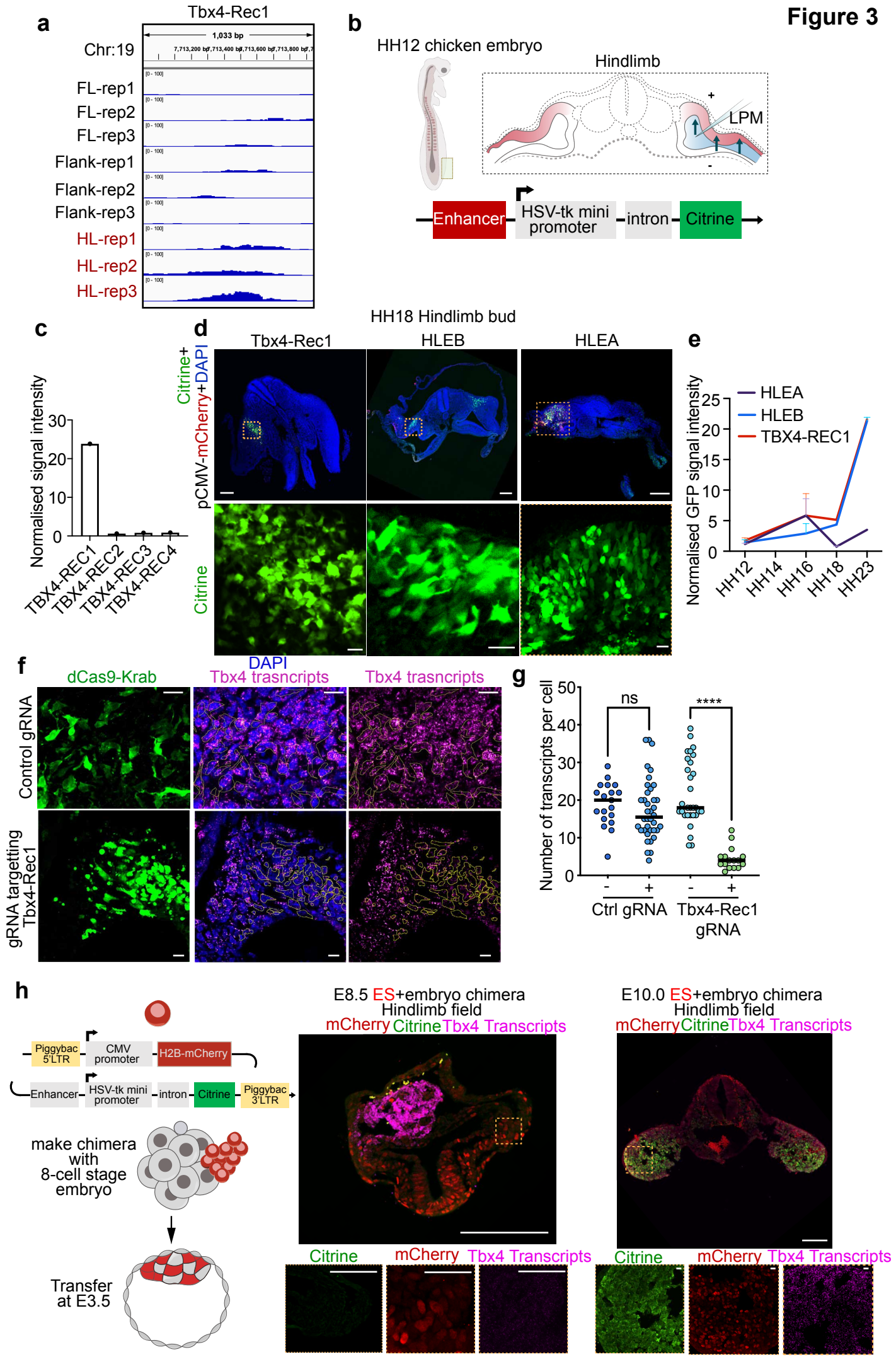
Figure 3
a
Tbx4-Rec1
1,033 bp
Chr:19
FL-rep1
FL-rep2
FL-rep3
Flank-rep1
Flank-rep2
Flank-rep3
HL-rep1
HL-rep2
HL-rep3
b
HH12 chicken embryo
Hindlimb
LPM
Enhancer
HSV-tk mini promoter
intron
Citrine
c
Normalised signal intensity
TBX4-REC1
TBX4-REC2
TBX4-REC3
TBX4-REC4
d
HH18 Hindlimb bud
Tbx4-Rec1
HLEB
HLEA
Citrine+ pCMV-mCherry+DAPI
Citrine
e
Normalised GFP signal intensity
HLEA
HLEB
TBX4-REC1
HH12
HH14
HH16
HH18
HH23
f
dCas9-Krab
DAPI
Tbx4 trasncripts
Tbx4 trasncripts
Control gRNA
gRNA targetting Tbx4-Rec1
g
Number of transcripts per cell
ns
****
Ctrl gRNA
Tbx4-Rec1 gRNA
h
Piggybac 5'LTR
CMV promoter
H2B-mCherry
Enhancer
HSV-tk mini promoter
intron
Citrine
Piggybac 3'LTR
make chimera with 8-cell stage embryo
Transfer at E3.5
E8.5 ES+embryo chimera
Hindlimb field
mCherry Citrine Tbx4 Transcripts
E10.0 ES+embryo chimera
Hindlimb field
mCherry Citrine Tbx4 Transcripts
Citrine
mCherry
Tbx4 Transcripts
Citrine
mCherry
Tbx4 Transcripts

Figure 4

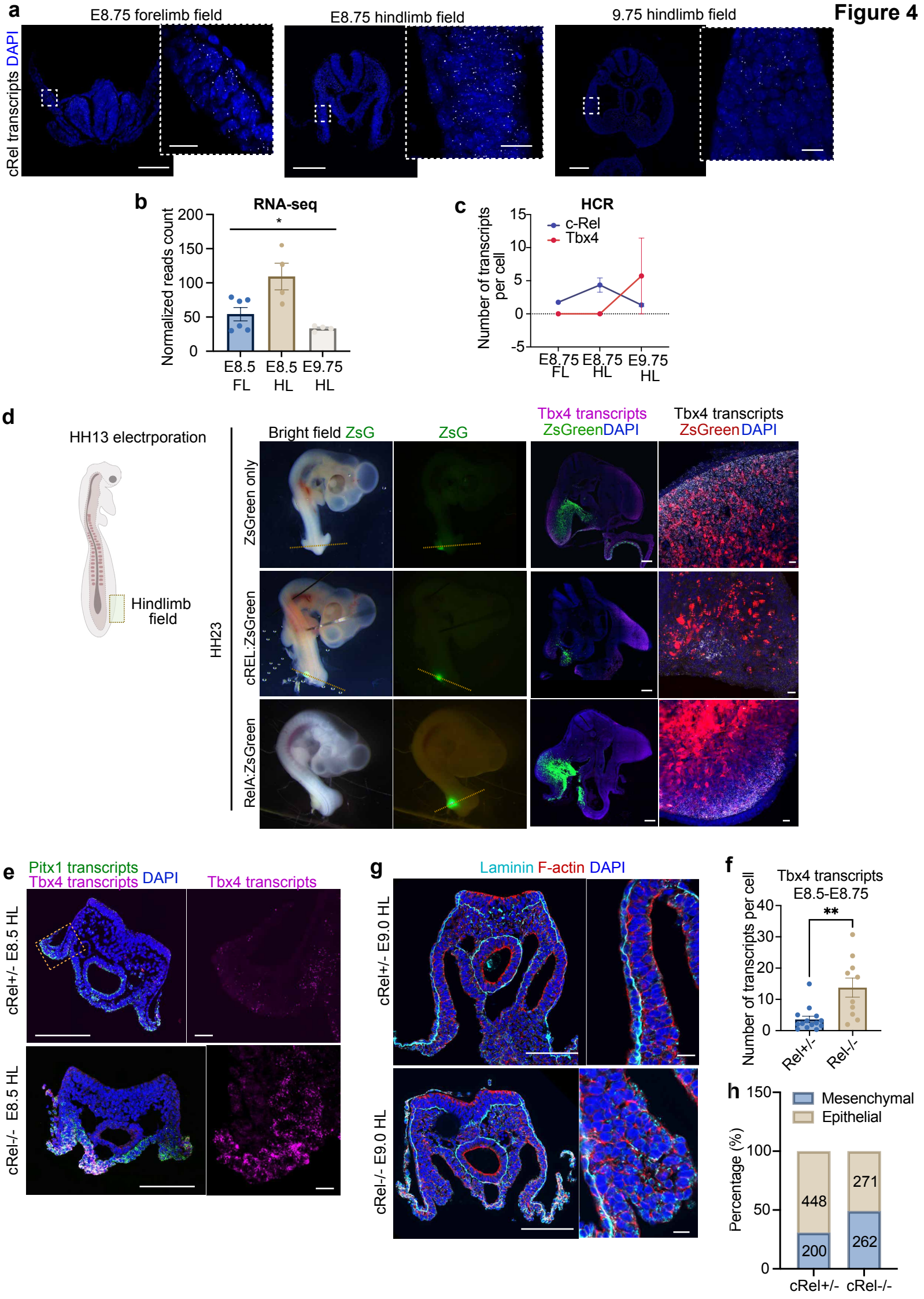
a
E8.75 forelimb field
E8.75 hindlimb field
9.75 hindlimb field
cRel transcripts DAPI
b
RNA-seq
Normalized reads count
200
150
100
50
0
*
E8.5 FL
E8.5 HL
E9.75 HL
c
HCR
Number of transcripts per cell
15
10
5
0
-5
c-Rel
Tbx4
E8.75 FL
E8.75 HL
E9.75 HL
d
HH13 electrporation
Hindlimb field
HH23
Bright field ZsG
ZsG
Tbx4 transcripts ZsGreenDAPI
Tbx4 transcripts ZsGreen DAPI
ZsGreen only
cREL:ZsGreen
RelA:ZsGreen
e
Pitx1 transcripts Tbx4 transcripts DAPI
Tbx4 transcripts
cRel+/- E8.5 HL
cRel-/- E8.5 HL
g
Laminin F-actin DAPI
cRel+/- E9.0 HL
cRel-/- E9.0 HL
f
Tbx4 transcripts E8.5-E8.75
Number of transcripts per cell
40
30
20
10
0
**
Rel+/-
Rel-/-
h
Mesenchymal
Epithelial
Percentage (%)
150
100
50
0
448
200
271
262
cRel+/-
cRel-/-

Figure 5

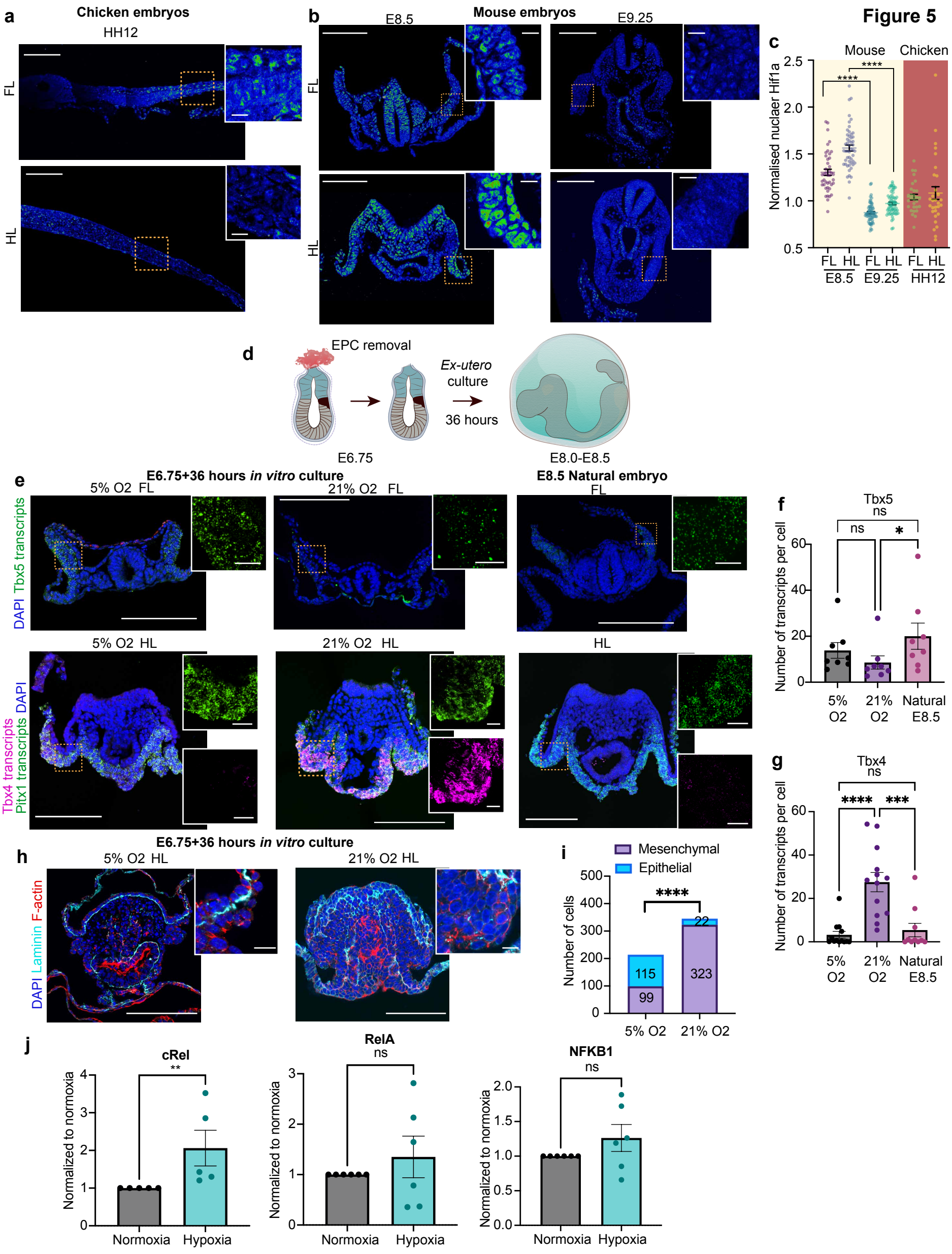
a
Chicken embryos
HH12
FL
HL
b
Mouse embryos
E8.5
E9.25
FL
HL
c
Mouse
Chicken
Normalised nuclaer Hif1a
****
****
FL HL FL HL FL HL
E8.5 E9.25 HH12
d
EPC removal
Ex-utero culture
36 hours
E6.75
E8.0-E8.5
e
E6.75+36 hours in vitro culture
E8.5 Natural embryo
5% O2 FL
21% O2 FL
FL
DAPI Tbx5 transcripts
5% O2 HL
21% O2 HL
HL
Tbx4 transcripts Pitx1 transcripts DAPI
f
Tbx5
ns
ns
*
Number of transcripts per cell
5% O2
21% O2
Natural E8.5
g
Tbx4
ns
****
***
Number of transcripts per cell
5% O2
21% O2
Natural E8.5
h
E6.75+36 hours in vitro culture
5% O2 HL
21% O2 HL
DAPI Laminin F-actin
i
Mesenchymal
Epithelial
****
Number of cells
115
99
323
22
5% O2
21% O2
j
cRel
**
RelA
ns
NFKB1
ns
Normalized to normoxia
Normoxia
Hypoxia

Figure 6

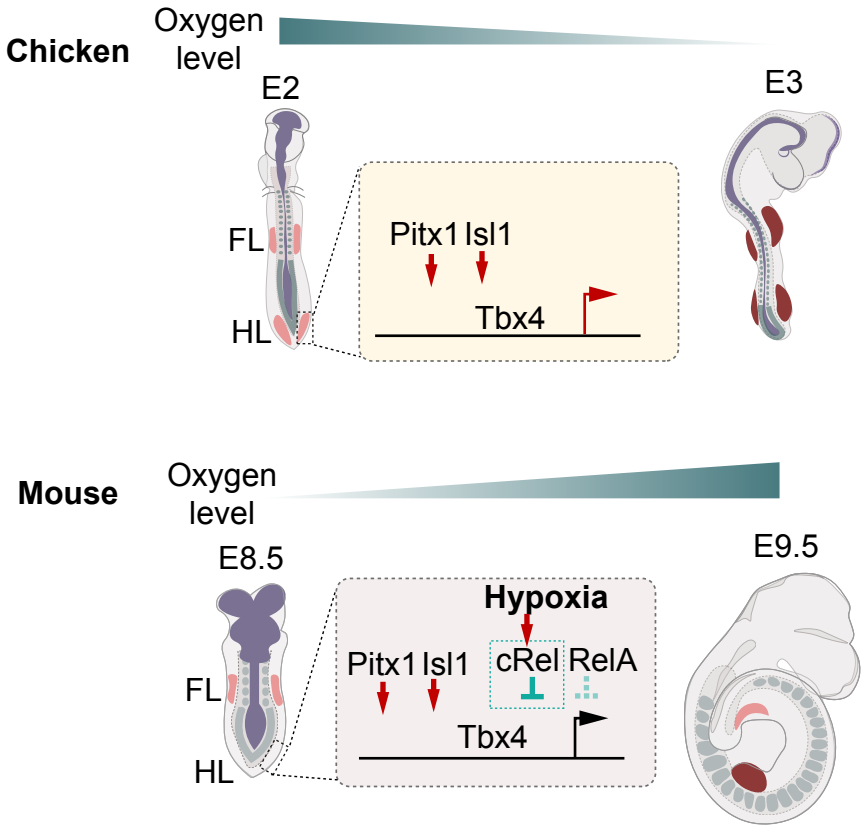
Chicken
Oxygen level
E2
E3
FL
HL
Pitx1 Isl1
Tbx4
Mouse
Oxygen level
E8.5
E9.5
FL
HL
Hypoxia
Pitx1 Isl1
cRel
RelA
Tbx4

Materials and Methods

Animals and husbandry

Mice with various backgrounds were maintained and manipulated under the regulations of IACUC. Wildtype lines, including CD1, C57BL/6J and F1 (mice are purchased from Charles River. cRel mutant line was imported from Stephen Smale lab (UCLA) and was described before(*1*). Tbx4 knockout line was purchased from Jackson Laboratory and was described previously(*2*). Fertilized chicken eggs were ordered from Charles River farm and incubated at 38℃ with 40% humidity.

Hybridization chain reaction (HCR)

Chicken embryos at HH8-HH23 stages and mouse embryos at E7.5-E10.0 stages were fixed in 4% PFA for 2h in room temperature or overnight at 4℃. Embryos were washed in PBST(PBS+0.1%Tween) for three times with 5mins each, and permeabilized in 70% ethanol in PBST for 2-5h at room temperature. The embryos were then washed by 37℃ pre-warmed washing buffer (Molecular Instruments co.) for 5mins and pre-hybridized in pre-warmed hybridization buffer (Molecular Instruments co.) for 30mins in 38℃ and then hybridized with hybridization buffer containing 60nM probes of targeted genes in 38℃ overnight. On the next day, the embryos were washed in pre-warmed washing buffer for two times with 30mins each time, followed by two times washes in 5xSSCT (5xSSC with 0.1% Tween) with 30mins each time. Embryos were pre-amplified in amplification buffer (Molecular Instruments co.) for 5mins at room temperature and then amplified in amplification buffer containing 48nM amplifiers matching the amplification sequences of each probe set. Before amplification, the amplifiers were heated in 95℃ for 90s and cooled down at room temperature for 30mins. The probes were designed following previous instructions.

Chicken embryo electroporation and Early Chick (EC) culture

For HH13 lateral plate mesoderm electroporation, the chicken embryos were incubated for 50 hours, after which 5 ml albumin was removed from each egg and then windowed on the top. The electroporation was performed as previously described(*3*). Briefly, plasmids with 1μg/ul mixed with FastGreen dye (0.2%) was injected into the coelom between two layers of lateral plate mesoderm of the forelimb or hindlimb and electroporated using BTX platinum needle L-shaped electrodes (45-0509). The electroporation was performed at 35 V, 5-ms pulse, 10-ms interval and 3-5 pulses. For HH4 chicken embryo electroporation, the eggs were cracked in 50-mm petri dishes and the albumin on the top of the embryo was gently removed using the blunt end of the forceps. The embryos were then transferred using pored filter papers (Whatman No.2) and was electroporated using Petri Dish Platinum Electrode using the following setting: 4 V, 50-ms pulse, 100-ms interval and 5 pulses. The embryos were then transferred to 35-mm petri dish coated with albumin+0.6% bacto agar supplemented with 15 mg glucose and 121 mM sodium chloride (NaCl). The embryos were then cultured in 38 ℃ for 24 hours.

Immunostaining

The chicken or mouse embryos were first fixed in 4% PFA for 2h in room temperature or overnight at 4℃. The embryos were then dehydrated in 30% sucrose and embedded in 50% OCT in 15% sucrose solution and then processed with cryostat sectioning. The OCT in sections were washed by PBS for two times and then blocked by TNB solution (150 mM NaCl, 100 mM Tris-HCl (pH=7.5), 0.3% Triton X-100, 0.5% blocking reagent (Roche, 11096176001)) for 30mins at room temperature, and then incubated with TNB solutions containing primary antibodies in 4C for overnight. For Hif1a staining, primary antibody was diluted in PBS. The slides were then washed for 3x5mins in PBS and incubated with 2nd antibodies for 1h at room temperature. After 2nd antibody incubation, PBS or PBS containing DAPI and F-actin (diluted in 1:1000) were incubated for 5mins, followed by PBS wash for 5mins and mounted with Invitrogen™ Fluoromount-G™ Mounting Medium covered by cover slides. Dilutions for primary antibodies: Rabbit Anti-Laminin

polyclonal antibody (Sigma-Aldrich, L9393), 1:500. Rabbit anti-HIF1a Polyclonal Antibody (Proteintech, 20960-1-AP), 1:100. Rabbit anti-phospho-Smad1 (Ser463/465)/ Smad5 (Ser463/465)/ Smad9 (Ser465/467) (D5B10) monoclonal antibody (Cell Signaling Technology, 13820S), 1:200. Secondary antibodies are diluted in TNB at 1:500 dilutions. List of antibodies include: donkey anti-Rabbit 488 (Jackson ImmunoResaerch, 711-545-152), donkey anti-Rabbit 568(Invitrogen, A10042), donkey anti-Rabbit 647 (Jackson ImmunoResaerch, 711-605-152).

Plasmids construction

Enhancer:reporter constructs: for constructing enhancer:reporter plasmids, pTK-RetE1-Citrine construct (a gift from Tatjana Sauka-Spengler (Addgene plasmid # 127779)) was double digested by KpnII (NEB, #R3142) and XmaI (NEB, R0180S) enzymes to create pTK-Citrine. Enhancer candidate regions were PCR amplified from chicken genomic DNA, with 5' and 3' primers carrying 18-22nt homologous sequences overlapping with the upstream and downstream of KpnI and XmaI sites of pTK--Citrine construct. The enhancer candidate regions were then cloned into pTK-Citrine vector via Gibson assembly. Positive clones were selected by both enzyme digestion and DNA sanger sequencing. The plasmids were maxi-preped before electroporation. Primers used for cloning are listed in Table S2.

Overexpression construct: pCAGGS-T2A-IRES-ZsGreen construct was double digested with XhoI (NEB, R1046) and EcoRI (NEB, R3101) enzymes. The protein coding sequence of cREL were amplified from chicken HH23 forelimb and hindlimb cDNA. 5' and 3' primers carrying 18-22nt homologous sequences overlapping with the upstream and downstream of XhoI and EcoRI sites of pCAGGS-T2A-IRES-ZsGreen construct. The coding sequences of genes of interest were then cloned into the construct via Gibson assembly. Positive clones were selected by both enzyme digestion and DNA sanger sequencing. The plasmids were maxi-preped before electroporation. The following primers are used:

***Ex-utero* culture**

E6.5 embryos were recovered from CD1 females mated with either CD1 or CB6F1 males, and were cultured in the medium containing 50% heat-inactivated rat serum (Biomed), 5% Fetal Bovine Serum 1× glutamax (GIBCO, 35050061), 100 units/ml penicillin and 100 μg/ml streptomycin (Biological Industries; 030311B) and 11mM HEPES (GIBCO, 15630056). Up to 3 embryos were placed in 12-well plate containing 2 ml medium each well. For each experiment, the embryos from the same batch were split into two groups and cultured for up to 2 days in 5% or 20% O_2 levels.

Real-time quantitative PCR (RT-qPCR)

RNA was extracted from dissected hindlimb field of ex-utero cultured embryos from E6.5+1.5 days, under 5% or 20% O_2, using the Arcturus PicoPure RNA isolation kit (Arcturus Bioscience). RT-PCR was performed using a StepOne Plus Real-time PCR machine (BioRad). The expression level was calculated using ddCT methods, normalized to a Atp5f2 PCR reaction and the endogenous control group. The primers used for RT-PCR are as below (all targeting mouse RNA sequences): Atp5f1-F: AGTTCCTTTACCCTAAGACTGGT; Atp5f1-R: TTCATGCTCGACTGCTTTACTT. cRel-F: ACAACAACCGGACATACCCG; cRel-R: GGTCTGCGTTCTGGTCCAA. RelA-F: AGCGCGGGGACTATGACTT; RelA-R: GCCCGGTTATCAAAAATCGGAT. Nfkb1-F: ATGGCAGACGATGATCCCTAC; Nfkb1-R: CGGAATCGAAATCCCCTCTGTT. Nfkb2-F: TGGCATCCCCGAATATGATGA; Nfkb2-R: TGACAGTAGGATAGGTCTTCCG. RelB-F: GTTCCAGTGACCTCTCTTCCC; RelB-R: CCAAAGCCGTTCTCCTTAATGTA.

Making transgenic embryonic stem cells (ES)

Wild type E14 embryonic stem cells were transfected with two constrctus, that one codes super-piggybac transposases (NovoPro, V012800), and one contains piggybac LTRs enclosing three cassette: a) enhancer:reporter cassette that contains enhancer:Hsv-tk:Citrine; b) CMV:H2B-mCherry; 3) Eif1a: puroR. Two days after transfection, the positive clones were first selected by puromycin treatment at 1ug/ml. After a week, the cells were double selected by manually picking

the single cell formed colonies that do not show obvious citrine signal and detectable mCherry signal. Multiple clones were mixed and cultured together.

Making ES-embryo chimera

For making the chimera, F1 females (CB6F1, Charles River) were superovulated by PMSG injection on Day 1 and HCG injection on Day 3, and mated with F1 males to produce the embryos. The embryos were recovered at E1.5 and cultured until E2.5 in KSOM medium, on which day the zona pelluccida was removed by acid tyrode's solution. The transgenic ES cells were trypsinized into single cells, and aggregated with E2.5 mouse embryos before compaction. The chimeric embryos were then cultured in KSOM until E3.5, after which the chimeric embryos were transferred into the uterus of pseudo-pregnant CD1 females who were mated with sterilized CD1 males three days before the experiment. 20 chimeric embryos were transferred into each pseudo-pregnant female, and each experiment averagely 4 females were used for transfer.

Bulk RNA-sequencing and analyses

Tissues corresponding to the area of forelimb and hindlimb of chicken embryos at HH12, and mouse embryo at E8.5 and E9.5 were finely dissected and disassociated as single cell in TrypLE buffer. The RNA from each tissue was extracted using RNeasy Kit (Qiagen). 1ng of RNA was used for smart-seq v4 RNA sequencing. RNA was sequenced in pair-end. For the analyses, RNA sequencing reads were mapped to chicken genome Galgal6, and mouse genome mm10 by hisat2. FPKM (Fragments Per Kilobase per Million mapped reads) of genes were calculated by featureCounts, differentially expressed genes were calculated by DESeq2.

ATAC-seq identification of candidate CRE loci

The raw data deposited on GEO (GSE136775), as reported on Young et al (*Curr Biol* 2019 Nov 4;29(21):3681-3691.e5), was downloaded. After cleaning up and QC'ing the FASTQ files with TrimGalore (Krueger, 2015) and aligned them to the galGal6a (NCBI) genome using BWA (Li & Durbin, 2009), peaks were called with MACS2 (Zhang et al, 2008) using parameters recommended for ATAC-seq and genome coverage was determined using DeepTools (Ramirez

et al, 2016). Differential accessibility between hindlimb, forelimb, and flank were calculated using the BDGDIFF function within MACS2 (signal cutoff: 10^2).

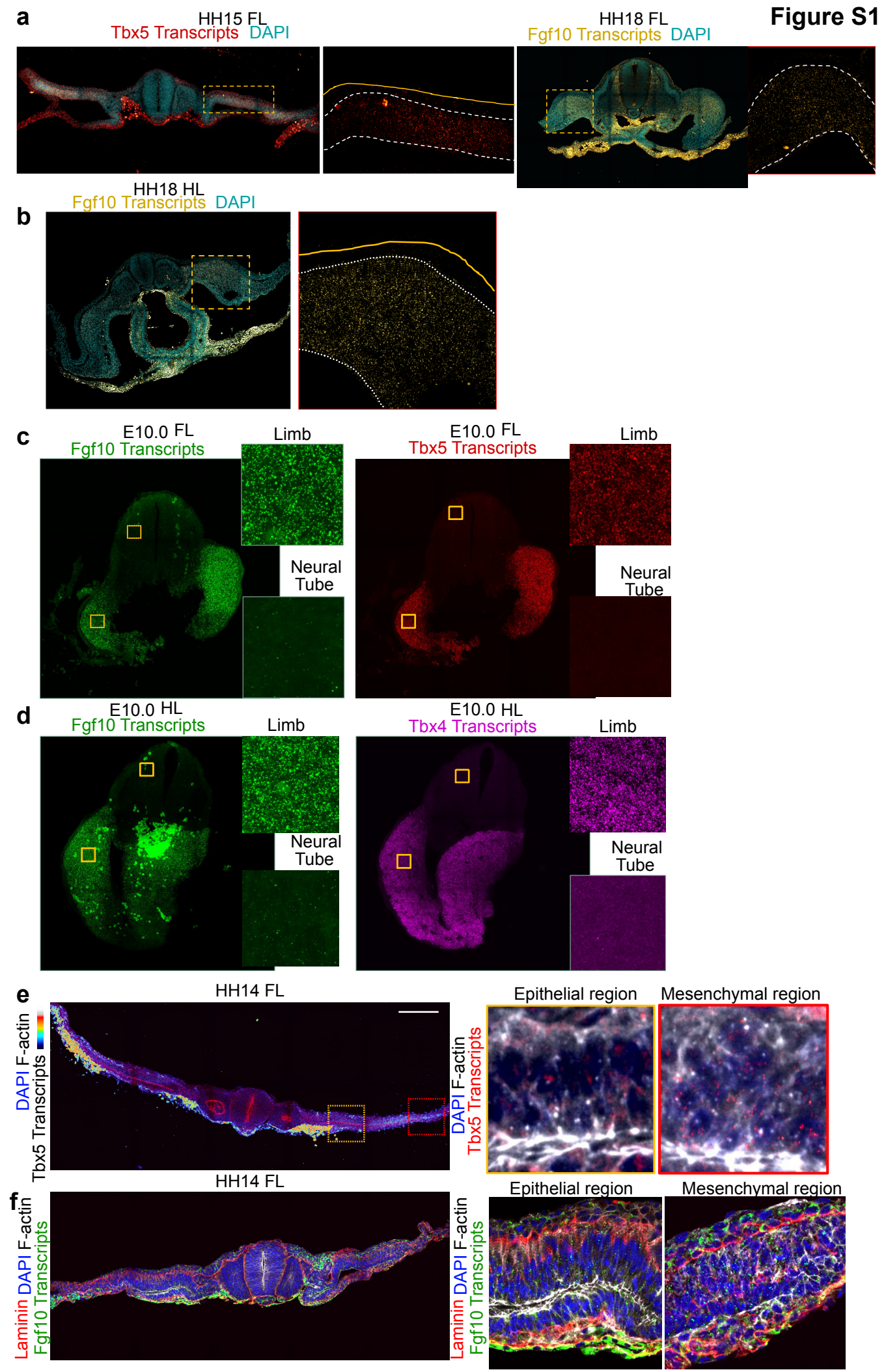
Figure S1
a
HH15 FL
Tbx5 Transcripts DAPI
HH18 FL
Fgf10 Transcripts DAPI
b
HH18 HL
Fgf10 Transcripts DAPI
c
E10.0 FL
Fgf10 Transcripts
Limb
Neural Tube
E10.0 FL
Tbx5 Transcripts
Limb
Neural Tube
d
E10.0 HL
Fgf10 Transcripts
Limb
Neural Tube
E10.0 HL
Tbx4 Transcripts
Limb
Neural Tube
e
HH14 FL
DAPI F-actin
Tbx5 Transcripts
Epithelial region
Mesenchymal region
DAPI F-actin
Tbx5 Transcripts
f
HH14 FL
Laminin DAPI F-actin
Fgf10 Transcripts
Epithelial region
Mesenchymal region
Laminin DAPI F-actin
Fgf10 Transcripts

Fig.S1. Expression of Tbx5 and Tbx4, but not Fgf10, correlate with the timing of EMT. (**a**-**b**) Visualization of Tbx5 in HH15 chicken forelimb, and visualization of FGF10 expression by HCR in forelimb (**a**) tissues and hindlimb (**b**) tissues of the chicken embryos at HH18. White dotted lines indicate magnified regions where yellow dotted lines indicate the region of LPM. N=5 embryos, N=4 experiments. (**c**) Visualization of Fgf10 and Tbx4 expression by HCR in E10.0 mouse forelimb tissue. (**d**) Visualization of Fgf10 and Tbx4 expression by HCR in E10.0 mouse hindlimb tissue. For **c**-**d**, yellow squares indicate magnified regions. N=6 embryos. N=3 experiments. (**e**) Correlation between TBX5 expression in chicken HH14 forelimb tissues by the Tbx5 transcripts visualized by HCR and F-actin and DAPI staining. Higher Tbx5 expression correlates with higher proportion of mesenchymal state. Quantification shown in Fig.1**h**. (**f**) No correlation between FGF10 transcripts levels and EMT in chicken HH14 forelimb tissues, as shown by the level of Fgf10 transcripts (visualized by HCR) and Laminin, F-actin and DAPI staining. For **e**-**f**, yellow dotted lines indicate proximal region where cells are mostly epithelial, dotted lines indicate distal region where cells are mostly mesenchymal. N=2 experiments, N=4 embryos. Scale bars for overview images, 150μm; scale bars for magnified images, 15μm.

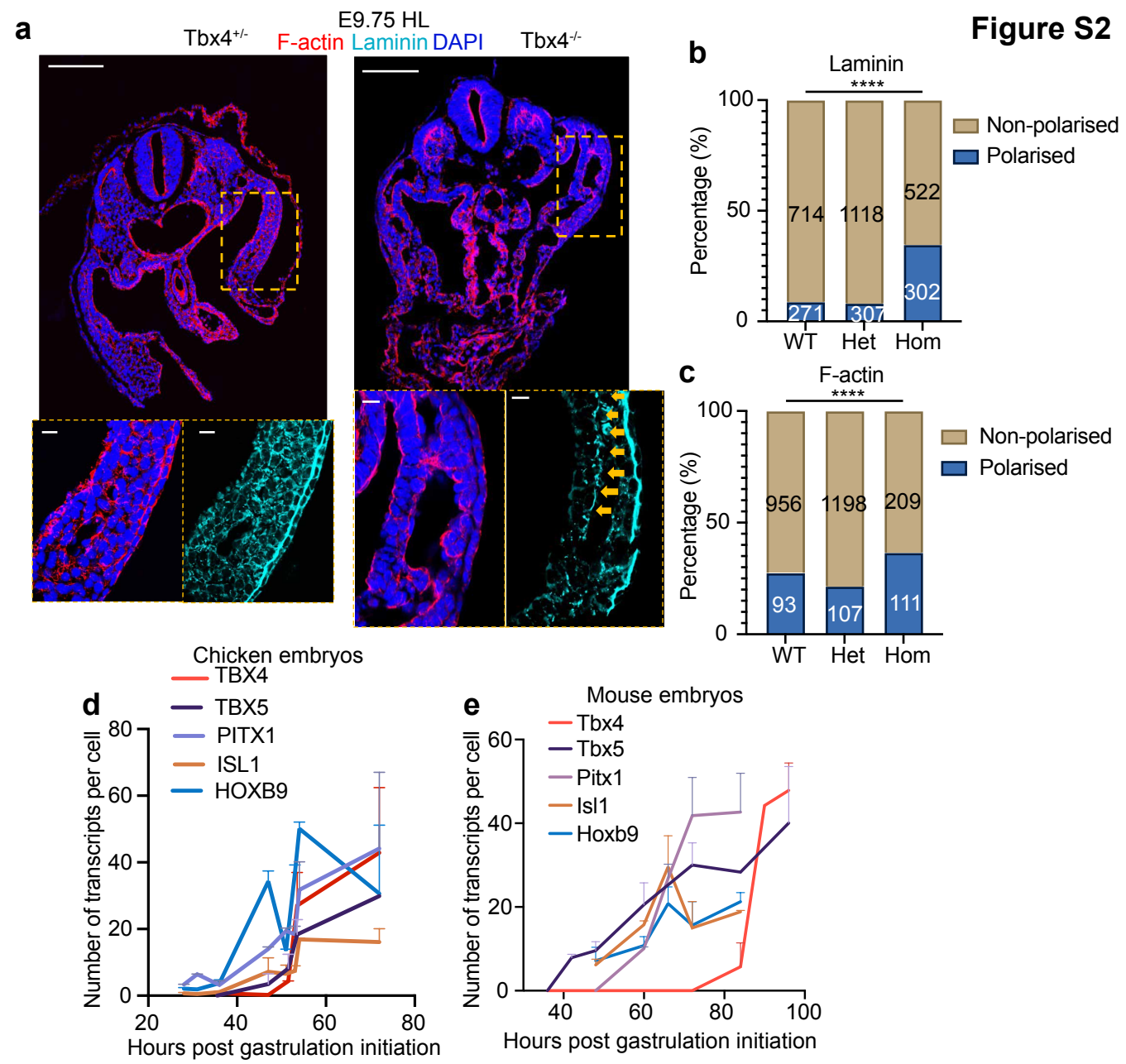
Figure S2
a
E9.75 HL
Tbx4+/-
F-actin Laminin DAPI
Tbx4-/-
b
Laminin
****
Percentage (%)
100
50
0
714
1118
522
271
307
302
WT
Het
Hom
Non-polarised
Polarised
c
F-actin
****
Percentage (%)
100
50
0
956
1198
209
93
107
111
WT
Het
Hom
Non-polarised
Polarised
Chicken embryos
d
TBX4
TBX5
PITX1
ISL1
HOXB9
Number of transcripts per cell
Hours post gastrulation initiation
Mouse embryos
e
Tbx4
Tbx5
Pitx1
Isl1
Hoxb9
Number of transcripts per cell
Hours post gastrulation initiation

Fig.S2. Tbx4 expression regulates hindlimb EMT and the delay of its expression is not regulated by the timing of Hoxb9, Pitx1 and Isl1 expression. (**a**) Cellular states in the hindlimb tissues of Tbx4 heterozygous and homozygous knockout embryos at E9.75. Dotted lines indicate magnified regions and the yellow arrows indicate epithelial cells that fail to undergo EMT on time and retained in the basal of hindlimb tissues in Tbx4 homozygous knockout embryos. N=6 embryos for Tbx4 heterozygous mutants and N=3 embryos for Tbx4 homozygous mutants. (**b**-**c**) Quantification of cells showing laminin (**b**) or F-actin (**c**) polarization as indications of epithelial state. The homozygous knockout embryos show higher proportion of epithelial cells comparing to wildtype (WT) or heterozygous embryos (Het). ****$p<0.0001$, Fisher's exact test. Data shown as bar charts with numbers in each bar represents the number of cells examined. N=3 embryos for WT, N=6 embryos for Het, and N=3 embryos for Hom. N=2 experiments. (**d**-**e**) Quantification of transcripts levels of Pitx1, Isl1 and Hoxb9 across HH8-HH18 in chicken embryos (**d**) and E7.5 to E10.0 in mouse embryos (**e**). The expression curves are aligned to that of Tbx5 and Tbx4, which reveals that while Hoxb9/Pitx1/Isl1 expression is almost concomitant with Tbx5 and Tbx4 in the chicken embryo, in the mouse embryo they only expression together with Tbx5, and Tbx4 expression is delayed. Data is shown as mean ± S.E.M. Scale bars for overview images, 150μm; scale bars for magnified images, 15μm.

Figure S3

a

Tbx4-Rec2

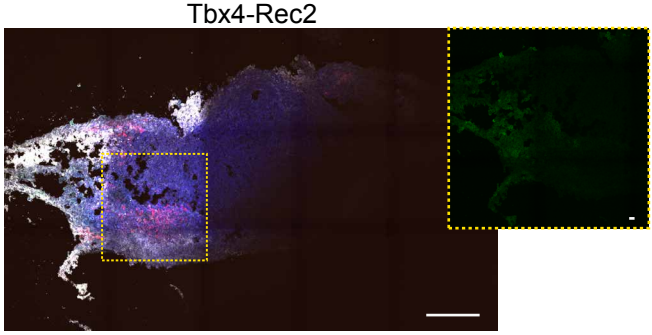

Tbx4-Rec3

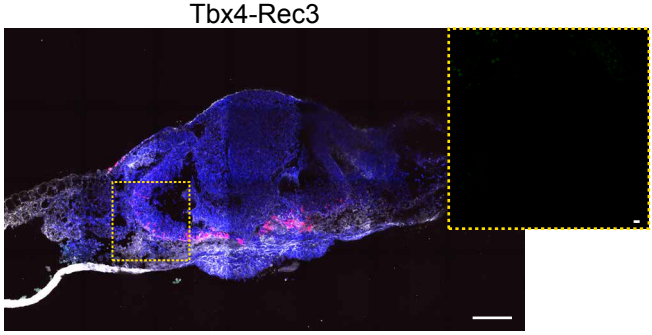

Tbx4-Rec4

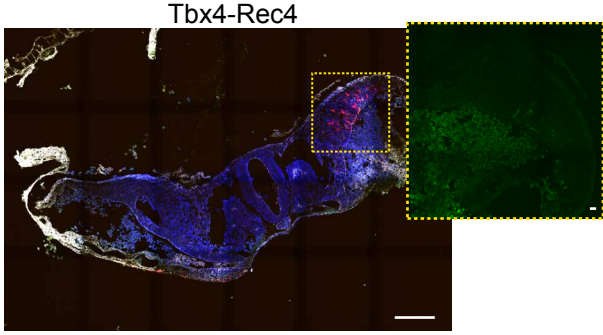

DAPI mCherry Citrine

b

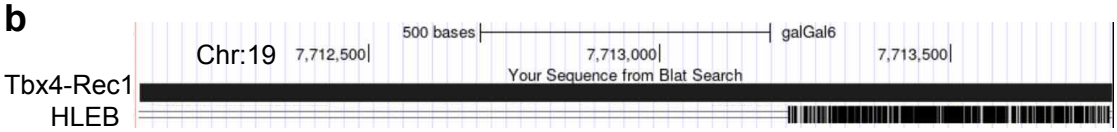

c

chimeric embryos E7.5
ES cells:mCherry

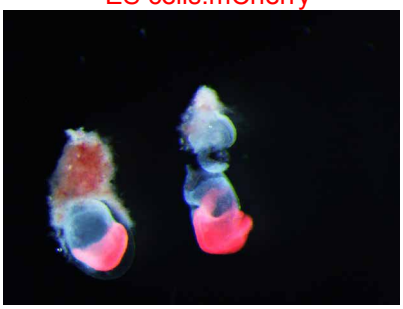

chimeric embryos E8.5
ES cells:mCherry

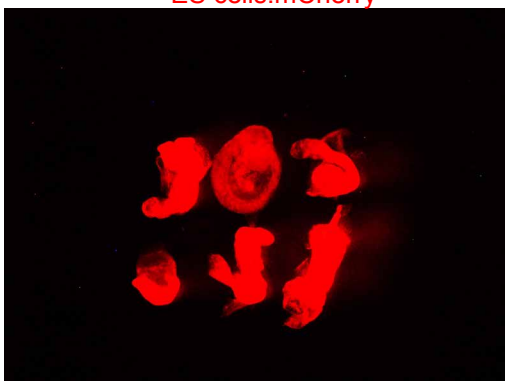

d

chimeric embryos E8.5 HL

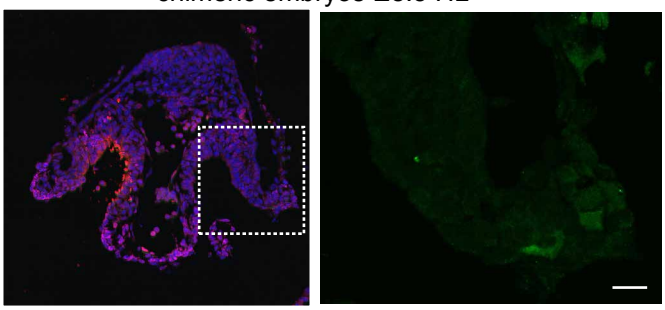

Citrine mCherry DAPI

e

chimeric embryos E9.75 FL

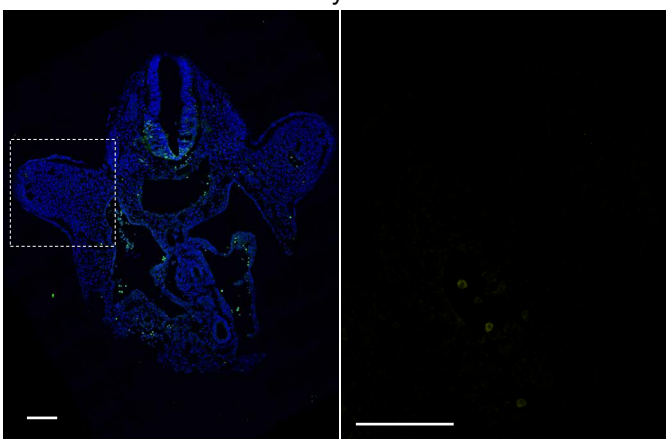

Citrine DAPI

chimeric embryos E9.75 HL

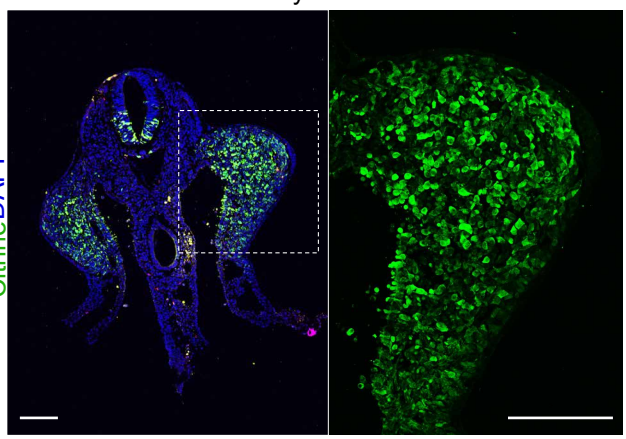

Citrine DAPI

Fig.S3. Chicken Tbx4 enhancer is conserved to that of mouse Tbx4 enhancer HLEB. (**a**) Enhancer:reporter constructs carrying Tbx4 enhancer candidate, Tbx4-Rec2, Tbx4-Rec3 and Tbx4-Rec4 were electroporated into the HH13 chicken embryos and the enhancer activity was examined at HH18 by Citrine signal. mCherry and DAPI were also revealed as electroporation and cell position control. Besides Tbx4-Rec1 (shown in Fig.3**d**), none of the other Tbx4 enhancer candidates show activities. Dotted lines indicate magnified regions. N=6 embryos for each construct, N=2 experiments. (**b**) Alignment of sequences between Tbx4-Rec1 and HLEB. 3' sequence of Tbx4-Rec1 show conservation to HLEB. The alignment is visualized through UCSC genome browser. Conservation score, 312. (**c**) Stereoscope images ES-embryo chimera dissected at E7.5 and E8.5. The transgenic ES cells are labelled with mCherry signal. Full penetration of the donor ES cells is achieved. (**d-e**) Chimeric embryos carrying HLEB:Citrine transgene was dissected at E8.5 (**d**) and E9.5 (**e**) to examine the enhancer activity as revealed by Citrine signal. Experimental workflow is shown in Fig.3**h**. White dotted lines indicate magnified regions. Scale bars for all images, 150μm.

Figure S4

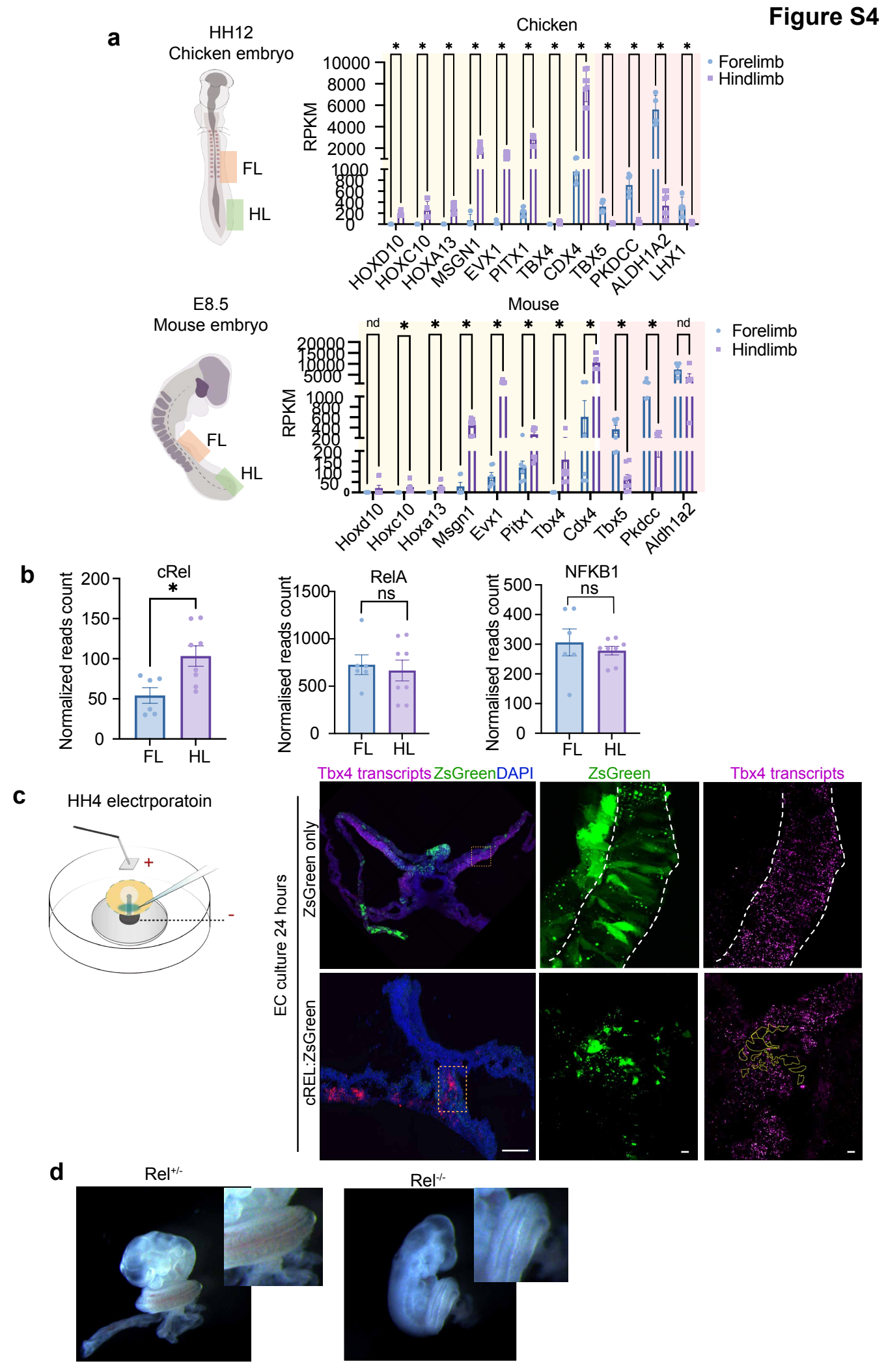
a
HH12
Chicken embryo
FL
HL
Chicken
RPKM
Forelimb
Hindlimb
HOXD10
HOXC10
HOXA13
MSGN1
EVX1
PITX1
TBX4
CDX4
TBX5
PKDCC
ALDH1A2
LHX1
E8.5
Mouse embryo
Mouse
nd
Hoxd10
Hoxc10
Hoxa13
Msgn1
Evx1
Pitx1
Tbx4
Cdx4
Tbx5
Pkdcc
Aldh1a2
b
cRel
RelA
NFKB1
ns
Normalized reads count
Normalised reads count
FL
HL
c
HH4 electrporatoin
Tbx4 transcripts
ZsGreen
DAPI
ZsGreen only
cREL:ZsGreen
EC culture 24 hours
d
Rel+/-
Rel-/-

Fig.S4. cRel represses the expression of Tbx4. (**a**) Bulk-RNA sequencing faithfully captures the transcriptional signatures of forelimb and hindlimb tissues at HH12 chicken embryo and E8.5 mouse embryo. (**b**) Expression levels of cRel, RelA and Nfkb1 in E8.5 mouse embryos and in forelimb and hindlimb fields from bulk-RNA seq shown in **a**. (**c**) Electroporation of CAG:cRel:ZsGreen overexpression constructs into the mesoderm and ectoderm of gastrulating chicken embryos at HH4 led to significant downregulation of Tbx4 in hindlimb field. Construct containing only ZsGreen was electroporated as a control. (**d**) cRel knockout embryos do not accelerate hindlimb bud formation at E9.5 and show similar hindlimb thickness as heterozygous littermates. N=4 embryos for heterozygous and N=4 for homozygous. (**e**) Quantification of the ratio of hindlimb/forelimb size in heterozygous and homozygous cRel mutants at E9.5. Data shown as mean± S.E.M. Each dot indicates an embryo. Scale bars for overview images, 150μm; scale bars for magnified images, 15μm.

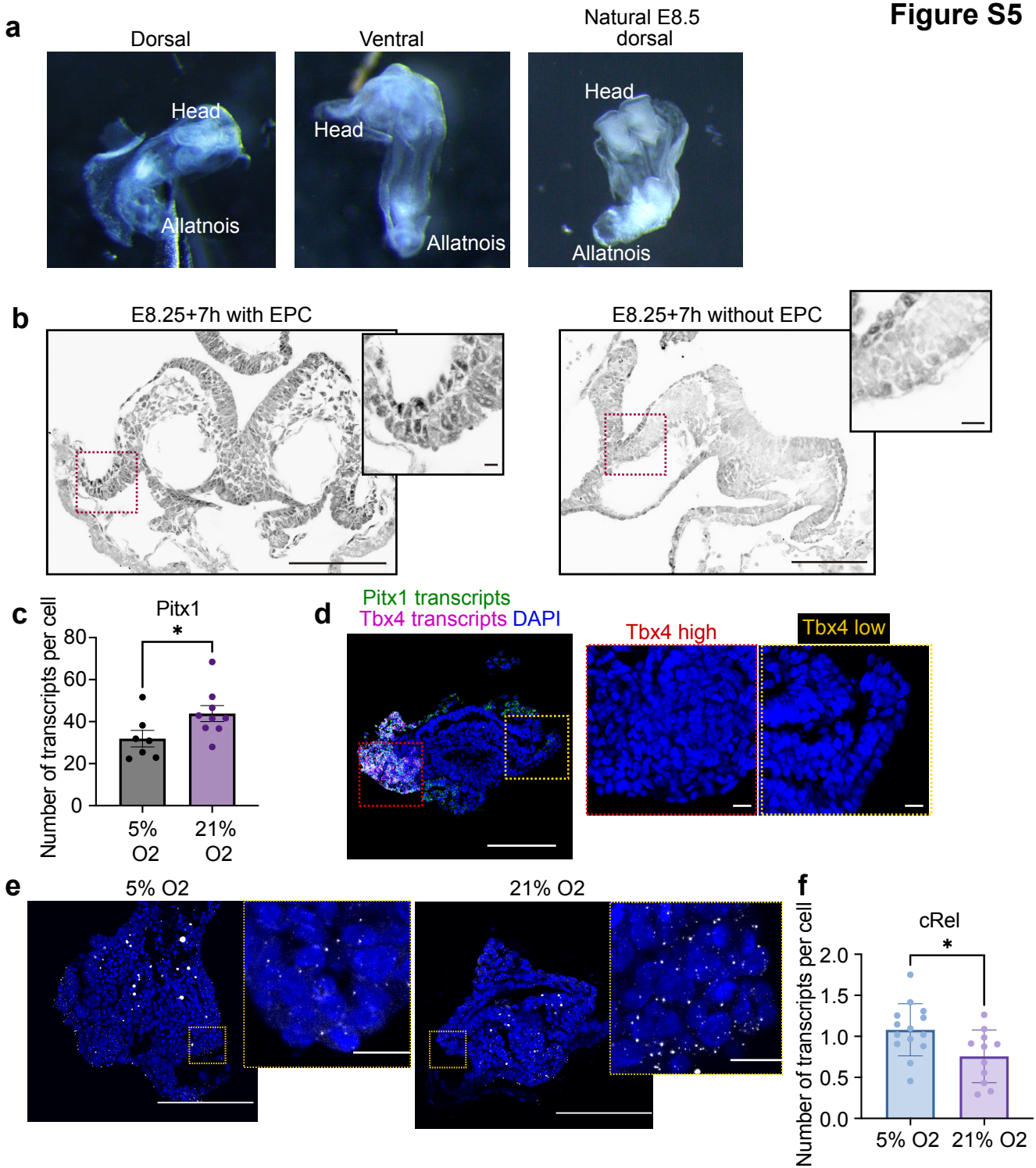
Figure S5
a
Dorsal
Ventral
Natural E8.5 dorsal
Head
Allatnois
Head
Allatnois
Head
Allatnois
b
E8.25+7h with EPC
E8.25+7h without EPC
c
Pitx1
*
Number of transcripts per cell
80
60
40
20
0
5% O2
21% O2
d
Pitx1 transcripts
Tbx4 transcripts DAPI
Tbx4 high
Tbx4 low
e
5% O2
21% O2
f
cRel
*
Number of transcripts per cell
2.0
1.5
1.0
0.5
0.0
5% O2
21% O2

Fig.S5. Ex-utero culture of embryos with prematurely elevated oxygen level show accelerated expression of hindlimb initiation regulators. (**a**) Gross morphology of embryos cultured in 5% O_2 using *ex-utero* culture method shown in Fig.5**d** and natural E8.5 mouse embryo. The morphologies of ex-utero cultured and natural E8.5 mouse embryos are similar expect that there were occasional defects in somite morphogenesis. N=22 experiments. (**b**) Removal of EPC facilitates higher efficiency of oxygen transportation as indicated by the downregulation of Hif1a in the posterior embryonic tissues of E8.25 embryos cultured ex-utero for 7h. Red dotted lines indicate magnified regions. N=2 sections from N=2 embryos. N=2 experiments. (**c**) *Ex-utero* culture of embryos (protocol shown in Fig.5d) in normoxia led to significant upregulation of Pitx1 in hindlimb tissues. *$p<0.05$, Student's t test. Each dots indicate one embryo. N=8 experiments for both 5% and 20% O_2. (**d**) Expression of Tbx4 correlate with cell number and epithelial/mesenchymal state as revealed by the expression of Pitx1 and Tbx4 transcripts (by HCR) and the staining of DAPI. Red dotted line indicates region that highly express Tbx4 (more cell numbers and multi-layer of cells) and yellow dotted line indicates the region that show no Tbx4 expression (less cell numbers and mono-layer of cells). Scale bars for overview images, 150μm; scale bars for magnified images, 15μm.

Table S1. List of genes selected for functional analysis. 22 genes were selected from RNA-sequencing analysis and were overexpressed into the lateral plate mesoderm of HH4 or HH13 chicken embryos to examine the effect on Tbx4 expression.

ZBTB16
COX4L1
PLA2G7
cREL
EVX1
MYC
NAAA
HOXD11
ZFP488
RIPK3
ETV4
ETV5
RBP1
CYSTM
SFN
LMBR1
TNFRSF11A
MECOM
PDGFC
PRRX2
RET

Table S2. Primers for cloning genes for overexpression assay. Primers are designed to amplify protein-coding region of each gene and are compatible for conduct Gibson assembly.

Sequence name	Sequence
XhoI-NAAA-F	CAAAGAATTACGCGTGCTAGCTCGAGCTCCGGCGGCGATGC
EcoRI-NAAA-R	GGGGCGGATCCCATCTAGAATAGTCAGCATGTTATTTACTCCACTTCATAGTTC
XhoI-ETV4-F	CAAAGAATTACGCGTGCTAGCTCGAGATGAAGGGGTACGTGGACCAG
EcoRI-ETV4-R	GGGGCGGATCCCATCTAGAATCAGCAGCTCTAGTAGGTGTAGCC
XhoI-ZBTB16-F	CAAAGAATTACGCGTGCTAGCTCGAGGGGAGTGCTATGGATTTGACTAAGATGG
EcoRI-ZBTB16-R	GGGGCGGATCCCATCTAGAATTCCCTCAGACGTAGCAGAGGTAGAGATAG
XhoI-ETV5-F	CAAAGAATTACGCGTGCTAGCTCGAGATGGACGGCTTCTACGACCAG
EcoRI-ETV5-R	GGGGCGGATCCCATCTAGAATTCGCCATCAGTAGGCAAAGCCCTC
XhoI-TNFRSF11A-F0	CAAAGAATTACGCGTGCTAGCTCACAGAATCATAGAACATGCCGAGTGG
EcoRI-TNFRSF11A-R0	GGGGCGGATCCCATCTAGAATTCGCTCTCAGAAGAAACGAATCTGTCC
XhoI-SFN-F	CAAAGAATTACGCGTGCTAGCTCGAGATGGCAAGAAACCACCAGGTGC
EcoRI-SFN-r	GGGGCGGATCCCATCTAGAATTCGCCGTTCAGTTCTTGGGCTCTTCG
XhoI-LMBR1-F	CAAAGAATTACGCGTGCTAGCTCGAGGATGGAGGCGGACGAGGTG
EcoRI-LMBR1-R	GGGGCGGATCCCATCTAGAATTCGCTCTGTTGATTGCAGGTGATTGTC
XhoI-MECOM-F	CAAAGAATTACGCGTGCTAGCTCGAGAGATGCAGAGCCGTGCCAG
EcoRI-MECOM-R	GGGGCGGATCCCATCTAGAATTCGGTCCCATTCTTGGTAAGACTTCAC
XhoI-PDGFC-F	CAAAGAATTACGCGTGCTAGCTCGAGATGCTCCTCCTCGGGCTG
EcoRI-PDGFC-R	GGGGCGGATCCCATCTAGAATTCTGAGATTACAGAAGGAGATAATGCACAAGCC
XhoI-PRRX2-F	CAAAGAATTACGCGTGCTAGCTCGAGGGTGGGAGCCATGGACTCG
EcoRI-PRRX2-R	GGGGCGGATCCCATCTAGAATTCGGTCAGTTCACAGTCGGCACC
XhoI-RET-F	CAAAGAATTACGCGTGCTAGCTCGAGATGGGACTTCTCTACCTCAGCAAG

EcoRI-RET-R	GGGGCGGATCCCATCTAGAATTCCCTCGTGAGTCCATTACCTTTCAC
XhoI-cRIPK3-F	CAAAGAATTACGCGTGCTAGCTCGAGAGGCTGGACTGTAGTAAAGCCTTG
EcoRI-cRIPK3-R	GGGGCGGATCCCATCTAGAATTCGTAGCAAACCTCAAAATTATGTCACAGCAG
XhoI-cCYSTM1-F	CAAAGAATTACGCGTGCTAGCTCGAGCATCCCAAATGAACTACGAAAATCCTCC
EcoRI-cCYSTM1-R	GGGGCGGATCCCATCTAGAATTCCGTGAGAGGTACGGCAGCTC
XhoI-cREL-F	CAAAGAATTACGCGTGCTAGCTCGAGTCAGCATGGCGGGTATCTCAGAGC
EcoRI-cREL-R	GGGGCGGATCCCATCTAGAATTCGGCTCAATGGTTATAGCTTTGTAATATGTTTGTATC
XhoI-NAAA-F	CAAAGAATTACGCGTGCTAGCTCGAGCTCCGGCGGCGATGC
EcoRI-NAAA-R	GGGGCGGATCCCATCTAGAATAGTCAGCATGTTATTTACTCCACTTCATAGTTC
XhoI-ETV4-F	CAAAGAATTACGCGTGCTAGCTCGAGATGAAGGGGTACGTGGACCAG
EcoRI-ETV4-R	GGGGCGGATCCCATCTAGAATCAGCAGCTCTAGTAGGTGTAGCC
XhoI-ZBTB16-F	CAAAGAATTACGCGTGCTAGCTCGAGGGGAGTGCTATGGATTTGACTAAGATGG
EcoRI-ZBTB16-R	GGGGCGGATCCCATCTAGAATTCCCTCAGACGTAGCAGAGGTAGAGATAG
XhoI-cNOTUM-F	CAAAGAATTACGCGTGCTAGCTCGAGGGGCGGCGATGGGCAC
EcoRI-cNOTUM-R	GGGGCGGATCCCATCTAGAATTCGAGAAGGGCTCCGAGTCTCC
XhoI-cPla2g7-F	CAAAGAATTACGCGTGCTAGCTCGAGAACAAGTGATGGCATCGCTGTG
EcoRI-cPla2g7-R	GGGGCGGATCCCATCTAGAATTCCTTCCTTGTACTCCTTACTCAGTTGGAGATAAG
XhoI-COX4I1-F	CAAAGAATTACGCGTGCTAGCTCGAGGATGTTGGCTTCAAGAGCATTCAGC
EcoRI-COX4I1-R	GGGGCGGATCCCATCTAGAATTCGCAGGTTCCACTGAGTTGCTTC
XhoI-ggMyc-F	CAAAGAATTACGCGTGCTAGCTCGAGGCAATTATTGCCTCGCTCCGTC
EcoRI-ggMyc-R	GGGGCGGATCCCATCTAGAATGTATTCTAAGTGATGTCCAAGAGTTCCTATGC
XhoI-MsHoxd11-F	CAAAGAATTACGCGTGCTAGCTCGAGCCATGAACGACTTTGACGAGTGCG
EcoRI-MsHoxd11-R	GGGGCGGATCCCATCTAGAATTCCAGAGAAGAGGCGTCATTGAACC

Supplementary References

51. F. Kontgen *et al.*, Mice lacking the c-rel proto-oncogene exhibit defects in lymphocyte proliferation, humoral immunity, and interleukin-2 expression. *Genes Dev* **9**, 1965-1977 (1995).
52. L. A. Naiche, V. E. Papaioannou, Loss of Tbx4 blocks hindlimb development and affects vascularization and fusion of the allantois. *Development* **130**, 2681-2693 (2003).
53. N. L. Nerurkar, C. Lee, L. Mahadevan, C. J. Tabin, Molecular control of macroscopic forces drives formation of the vertebrate hindgut. *Nature* **565**, 480-484 (2019).